Philosophical Magazine

ISSN: 1478-6435 (Print) 1478-6443 (Online) Journal homepage: http://www.tandfonline.com/loi/tphm20

On the temperature independence of statistical model parameters for cleavage fracture in ferritic steels

Guian Qian, Wei-Sheng Lei, M. Niffenegger & V. F. González-Albuixech

To cite this article: Guian Qian, Wei-Sheng Lei, M. Niffenegger & V. F. González-Albuixech (2018): On the temperature independence of statistical model parameters for cleavage fracture in ferritic steels, Philosophical Magazine, DOI: 10.1080/14786435.2018.1425011

To link to this article: https://doi.org/10.1080/14786435.2018.1425011

PHILOSOPHICAL MAGAZINE, 2018
https://doi.org/10.1080/14786435.2018.1425011

Taylor & Francis
Taylor & Francis Group

On the temperature independence of statistical model parameters for cleavage fracture in ferritic steels

Guian Qian[a‡], Wei-Sheng Lei[b], M. Niffenegger[a] and V. F. González-Albuixech[c]

[a]Nuclear Energy and Safety Department, Laboratory for Nuclear Materials, Paul Scherrer Institute (PSI), Villigen, Switzerland; [b]Applied Materials, Inc., Sunnyvale, CA, USA; [c]CIIM Universitat Politècnica de València, Camino de Vrea, Valencia, Spain

ABSTRACT

The work relates to the effect of temperature on the model parameters in local approaches (LAs) to cleavage fracture. According to a recently developed LA model, the physical consensus of plastic deformation being a prerequisite to cleavage fracture enforces any LA model of cleavage fracture to observe initial yielding of a volume element as its threshold stress state to incur cleavage fracture in addition to the conventional practice of confining the fracture process zone within the plastic deformation zone. The physical consistency of the new LA model to the basic LA methodology and the differences between the new LA model and other existing models are interpreted. Then this new LA model is adopted to investigate the temperature dependence of LA model parameters using circumferentially notched round tensile specimens. With the published strength data as input, finite element (FE) calculation is conducted for elastic-perfectly plastic deformation and the realistic elastic-plastic hardening, respectively, to provide stress distributions for model calibration. The calibration results in temperature independent model parameters. This leads to the establishment of a 'master curve' characteristic to synchronise the correlation between the nominal strength and the corresponding cleavage fracture probability at different temperatures. This 'master curve' behaviour is verified by strength data from three different steels, providing a new path to calculate cleavage fracture probability with significantly reduced FE efforts.

ARTICLE HISTORY
Received 30 June 2017
Accepted 31 December 2017

KEYWORDS
Ferritic steels; plastic yielding; cleavage fracture; statistical model; temperature effect; model calibration

1. Introduction

A framework for statistical modelling of plastic yielding initiated cleavage fracture of structural steels [1] was recently published to extend a new local approach (LA) model proposed in [2] to the more generic cases, such as including different distributions of microcracks. The present work is an effort to validate this framework

CONTACT Wei-Sheng Lei Wei-Sheng_Lei@amat.com, Leiws2008@gmail.com
‡State Key Laboratory for Nonlinear Mechanics (LNM), Institute of Mechanics, Chinese Academy of Sciences, Beijing, China.

using some published data-sets on cleavage fracture. More specifically, it is targeted to validate the temperature independence of model parameters using notched specimens. The framework also suggested the stress state independence of model parameters, the validation of which will be reported separately. To begin with, we will highlight some most closely related aspects as background information, with an emphasis on elaborating the major differences between the new LA model and some typical LA models. The reader is referred to [1–3] for an in-depth critical review on existing LA models for cleavage fracture. Following a brief introduction to the new LA model in Section 2, the physical consistency of the new LA model to the basic LA methodology and the differences between the new LA model and other LA models are summarised in Section 3.

Ferritic low alloy steels are commonly used in the fabrication of many key engineering structures with very stringent reliability requirements. For example, reactor pressure vessels (RPVs) are the most critical components of a nuclear power plant [4,5]. Today, essentially all the RPVs in the commercial light water reactors are made of ferritic low alloy steels. The body centred cubic crystal structures of ferritic steels endow them with the inherent susceptibility to cleavage fracture. Cleavage fracture is a random event and can lead to catastrophic structural failures. Extrinsically, the randomness of cleavage fracture is manifested by a large variation of fracture toughness values measured on a group of nominally identical specimens under same testing conditions at a same temperature and by a pronounced specimen geometrical constraint dependence of fracture toughness. Intrinsically, the random occurrence of cleavage fracture is attributed to the stochastic distribution of the potential cleavage cracking initiators (e.g. carbides, martensite–austentie (M–A) constituents, and other second-phase brittle particles) in terms of their spatial location, orientation, shape and size in combination with the randomly orientated cleavage planes, which are well-defined, low-index crystallographic planes of matrix ferrite grains in polycrystalline steels. The ever stringent safety requirement for key engineering structures such as RPVs and the random characteristics of cleavage fracture inherent to ferritic steels inevitably call for physically consistent and mathematically rigorous statistical approaches, often known as the LAs, for cleavage fracture assessment. The efforts on statistical modelling of cleavage fracture date back to the early 1980s [6,7] and from then on have actively continued [1,2,8–17]. Essentially, all the LAs to cleavage fracture possess the following common features: (1). physically, the precedence of plastic yielding over cleavage fracture is observed as a consensus; In addition, the occurrence of cleavage fracture is dominated by the maximum principal tensile stress criterion; (2). mathematically, the weakest link postulate applies to cleavage fracture process; the cumulative failure probability is always formulated as a function of certain volume integral incorporating tensile stress distribution with certain model parameters to be calibrated. The reader is referred to Pineau [13] for a comprehensive review and Lei [1] for a detailed commentary on the LAs to cleavage fracture. Here, we will concentrate on elaborating the ambiguity of

model parameter calibration, which is the persistent critical challenge to LAs to cleavage fracture. In brief, the ambiguity of model parameter calibration refers to the much uncertainty and dependence of the calibrated model parameters on temperature, test piece geometry (shape and size), and loading condition (loading mode and speed).

Despite the differences of each specific LA model, it is commonly agreed that a statistical model of cleavage fracture is logically expected to unitedly characterise and predict the cleavage fracture behaviour of a given steel in different geometries (smooth, notched, and cracked specimens of different size), under different loading conditions (loading mode and loading rate), and at different temperatures. This is the exact point that distinguishes a predictive statistical model from a descriptive one. It naturally establishes the calibration of statistical model parameters as a critical step in the validation, justification and subsequent application of any statistical model with prediction capability. The logical requirement on the transferability or scalability of a statistical model between different test conditions (specimen geometry, temperature, and loading condition) demands the model parameters to be fairly consistent and be reliably calibrated without ambiguity. Otherwise, the model degenerates into a descriptive tool with much limited prediction power.

Take the Beremin model [7,13] for example. It is essentially a two-parameter Weibull distribution as below:

$$P = 1 - exp\left[-\left(\int_{V_{pl}} \sigma_1^m \cdot \mathrm{d}V/V_0\right)/\sigma_0^m\right] = 1 - \exp\left[-\left(\sigma_{W,Beremin}/\sigma_0\right)^m\right] \quad (1)$$

$$\text{with } \sigma_{W,Beremin} = \left(\int_{V_{pl}} \sigma_1^m \cdot \mathrm{d}V/V_0\right)^{1/m} \quad (2)$$

where P is the cumulative probability of failure, V_{pl} denotes the volume of the plastic deformation zone as the cleavage fracture process zone, m and σ_0 are the two model parameters known as Weibull modulus and the scale parameter, respectively, σ_1 is the maximum tensile principal stress, V_0 is an elementary volume representing the mean volume occupied by each micro-crack in a solid, dV is the differential volume.

Equation (1) was formulated due to the following two critical steps:

(1) The cumulative probability of failure (P) in a solid of volume V is described as

$$1 - P = \exp\left[-\int_V p(V_0)\frac{\mathrm{d}V}{V_0}\right] \quad (3)$$

where $p(V_0)$ is the fracture probability of an elementary volume (V_0) induced by an embedded microcrack under an arbitrary stress state.

(2) The size (a) distribution density function of micro-cracks induced by plastic deformation obeys a power law,

$$f(a) = \mu \cdot a^{-\kappa} \tag{4}$$

where μ and κ are material constants.

Due to the maximum tensile principal stress σ_1 fracture criterion, Equation (4) led to [7]:

$$p(V_0) = \int_{a_c(\sigma_1)}^{\infty} f(a)da = (\sigma_1/\sigma_0)^m \tag{5}$$

$$\sigma_0 = (m/2\mu)^{1/m} \sqrt{2E\gamma/(1-\nu^2)}, \quad m = 2\kappa - 2 \tag{6a,b}$$

where $a_c = 2E\gamma/\left[(1-\nu^2)\sigma_1^2\right]$ is the critical size of a penny-shaped microcrack according to the Griffith law, γ is the effective fracture surface energy of the matrix, E is Young's modulus and ν is Poisson's ratio.

The two model parameters (m and σ_0) in Equation (1) need to be calibrated numerically from a set of fracture experiments before any practical application. As shown in Equations (6a,b), m varies with the shape factor (κ) of microcrack size (a) distribution, and σ_0 depends on the elastic properties (E, ν), the surface energy of the material (γ), and the scale of microcrack size distribution (μ), which are less sensitive to plastic constraint or temperature. Therefore, m and σ_0 should be intrinsic material constants dependent exclusively on material microstructures and approximately independent of constraint and temperature. On the contrary, the calibrated values of m and σ_0 vary dramatically with temperature and specimen geometries and loading conditions. A typical example is the result of Beremin model calibration of a structural steel by Wiesner and Goldthorpe [8]: Within the temperature range from 143 to 77 K, m varies between 13 and 23 for round notched bar tensile specimens, ranges from 37 to 60 for the V-shape notched four-point bending specimens, and from 11 to 49 for the fracture mechanics specimens, along with significant variations of σ_0.

In order to resolve the ambiguous calibration of Beremin model, continuing efforts have been made along the following three technical paths to expand the Beremin model into the so-called Weibull stress models [10–13,15–17]:

(1) *Incorporating the plastic strain (ε_p) effect*. The Weibull stress σ_W is empirically modified to adopt the plastic strain (ε_p) correction:

$$\sigma_W = \left(\int_{V_{pl}} \sigma_1^m \cdot \mathrm{h}(\varepsilon_p) \cdot \mathrm{d}V/V_0 \right)^{1/m} \tag{7}$$

where $h(\varepsilon_p)$ is a function of the plastic strain (ε_p). See [7,11,15] for some suggested expressions of $h(\varepsilon_p)$. The adoption of $h(\varepsilon_p)$ in Equation (7) as well as the different expressions of $h(\varepsilon_p)$ is purely empirical and lacks strict mathematical derivation as in Beremin model (from Equation (1) to Equation (6a,b)).

(2) *Introducing a fixed-value threshold stress (σ_{th}) or a minimum Weibull stress $\sigma_{W,min}$.* The cumulative failure probability formulation is empirically modified to adopt a fixed-value threshold stress (σ_{th}) or a minimum Weibull stress $\sigma_{W,min}$ without strict theoretical derivation, such as :

$$p = 1 - \exp\left[-\left(\frac{\sigma_W - \sigma_{th}}{\sigma_0 - \sigma_{th}}\right)^m\right] \quad [10] \tag{8a}$$

$$p = 1 - \exp\left[-\left(\frac{\sigma_W - \sigma_{W,min}}{\sigma_0 - \sigma_{W,min}}\right)^m\right] \quad [11] \tag{8b}$$

$$p = 1 - \exp\left[-\left(\frac{\sigma_W^{m/4} - \sigma_{W,min}^{m/4}}{\sigma_0^{m/4} - \sigma_{W,min}^{m/4}}\right)^4\right] \quad [12] \tag{9}$$

Note that in Equations(8b) [11] and (9) [12], the minimum Weibull stress $\sigma_{W,min}$ corresponds to the threshold toughness of the material, $K_{\min}$, in the following three-parameter Weibull model of fracture toughness (K_{J_c}) in the ASTM standard test method E1921–02:

$$P\left(K_{J_c}\right) = 1 - \exp\left[-\left(\frac{K_{J_c} - K_{min}}{K_0 - K_{min}}\right)^4\right], \tag{10}$$

with $K_{min} = 20\ \text{MPa}\sqrt{m}$ for common ferritic steels regardless of crack-front length and temperature (K_0 is a temperature dependent scale parameter). Since at $K_{J_c} = K_{min}, P\left(K_{J_c}\right) = 0$ in Equation (10), which means cleavage fracture cannot occur, there has to be at $\sigma_W = \sigma_{W,min}, P = 0$ in Equations (8b) and (9) in order to keep mutual consistency of Equations (8b) and (9).

These modifications are problematic in the following aspects:

(1) In all the three cases, the Weibull stress σ_W is still calculated by Equation (2) or (7). Therefore, similar to Equation (7), Equations (8a,b) and (9) are empirical modifications rather than based on a presumed microcrack size distribution as in Equation (4). In other words, a strict mathematical derivation of Equations (7), (8a,b) and (9) from the basic weakest-link formulation Equation (3) does not exist. This is quite

Table 1. Summary of calibrated model parameters based on Equation (10) [10].

Steel	Specimen	T (K)	V_0 (mm^3)	m	σ_0 (GPa)	σ_{th} (GPa)
A508	RNB(shallow)	153		23	2.78	0.0
	RNB(shallow)	123	0.001	24	3.16	0.8
	RNB(sharp)	123		8	4.98	0.0
A533B	SEN(B)	103	0.01	4	8.75	3.25
			0.1	4	4.5	1.0

obvious for Equations (7) and (8a,b). As for Equation (9), it is more likely derived from Equation (10). As mentioned by Petti and Dodds [12], under plane-strain small scale yielding (SSY) conditions, the existence of self-similar fields with amplitudes dependent only on J-integral, or equivalently $K_J = \sqrt{EJ/(1-\nu^2)}$, leads to the following relationship:

$$\sigma_W^m = k_0 BJ^2 = k_0[(1-\nu^2)/E]^2 BK_J^4 \tag{11a}$$

More generically, a non-dimensional constraint function $g(M)$ is included to rewrite Equation (11a) as

$$\sigma_W^m = k_0[(1-\nu^2)/E]^2 BK_J^4 g(M) \tag{11b}$$

where B is crack-front length, k_0 is a constant coefficient. The combination of Equations (10) and (11a) yields Equation (9). The parameter $M \propto \sigma_{ys}/J_{avg}$ measures the constraint effect, J_{avg} is the through-thickness average value of J-integral. $g(M)$ characterises the amount of constraint loss once plane-strain, small scale yielding (SSY, with $M = 1$) conditions degenerate in specimens under increased plastic deformation. However, the proportional relationship revealed in Equations (11a,b) is based on the Beremin model, which, as shown in Equation (5), assumes an infinite value for the maximum microcrack size ($a_{max} = \infty$), or equivalently, $K_{min} = 0, \sigma_{th} = 0$. This is self-contradictory: On one hand, if we accept Equations (11a,b) as a valid relationship, the Beremin model will be justified, which yields the following well-known two-parameter Weibull model of fracture toughness [7,13]:

$$P\left(K_{J_c}\right) = 1 - \exp\left[-\left(\frac{K_{J_c}}{K_0}\right)^4\right], \tag{12}$$

As a result, Equation (10) should not hold true simultaneously with $K_{min} = 20\ \text{MPa}\sqrt{m}$. Consequently, Equation (9) would not exist. On the other hand, if we accept Equation (10) as a valid relationship, $K_{min} = 20\ \text{MPa}\sqrt{m}$ implies that $K_{min} \neq 0, \sigma_{th} \neq 0$. Then the Beremin model (Equation (5) or (12)) would be incorrect, hence the relationship in Equations (11a,b) based on the Beremin model should not be adopted, which makes the transformation from Equation (10) to Equation (9) unattainable.

The same argument on the incompatibility between $K_{min} \neq 0 (\sigma_{W,min} \neq 0)$ and the adoption of σ_W defined by the Beremin model in Equation (2) also applies to Equation (8b).

(2) As stated by Petti and Dodds [12], in contradiction to the basic assumption of Equation (10) that $K_{min} = 20\,\text{MPa}\sqrt{m}$ remains invariant of constraint variations, crack-front length, and temperature, 'the temperature dependence of K_{min} represents an open research issue at this time. Future work must address the effects of temperature on Kmin and the role in applications of the Weibull stress model'. Many studies such as [3] and [18] have analysed the temperature dependence of K_{min}. In addition, the value of σ_0 in Equations (8b) and (9) has to be adjusted with temperature in order to pursue the temperature independence of Weibull modulus m [11,12].This actually goes back to the fundamental concern on the applicable range of the Master Curve approach represented by Equation (10). As mentioned by Petti and Dodds [12],

> If the Master Curve actually does represent the toughness-temperature relation for the selected reference condition, the T_0 value (for the reference condition) would not change when computed at a different calibration test temperature (θ) using this procedure. Here, the computed T_0 values are 307, 313, and 318 K for the square, 1T-SE(B) reference condition for calibration temperature (θ) of 248, 298, and 328 K, respectively. For this material (A508 steel as a commonly used nuclear pressure vessel steel), the Master Curve apparently overpredicts the increase in toughness with temperature for a square 1T-SE(B) reference condition.

Since the determination of K_{min} at different temperatures involves a series of expensive experiments, if K_{min} remains a necessary input condition to enable the statistical modelling practice using Equations (8b) and (9), the presumed importance or even the necessity to develop statistical modelling of cleavage fracture is diluted significantly.

(3) The introduction of $\sigma_{W,min}$ at $K_{min} = 20\,\text{MPa}\sqrt{m}$ in Equations (8b) and (9) is applicable only for fracture mechanics specimens. In principle, a statistical model for cleavage fracture should be also applicable to notched specimens or other specimen geometries without a pre-crack. However, even for fracture mechanics specimens, as highlighted by Gao et al. [11], the value of $\sigma_{W,min}$ needs to be adjusted to accommodate intrinsic differences in the length of crack. For plane-strain, SSY conditions, $\sigma_{W,min} \propto B^{1/m}$, where B is specimen thickness (or crack-front length); for surface crack specimens, $\sigma_{W,min} \propto L^{1/m}$, where L is the length of the semi-elliptical crack front. The geometrical constraint in a notched or un-cracked specimen is much different from that in a pre-cracked specimen, it remains a mystery on how to determine the value of $\sigma_{W,min}$ for a specimen without a pre-crack. Consequently, it is unclear how to apply Equations (8b) and (9) to specimens without a pre-crack.

(4) As elaborated in detail in [3], the determination of the threshold σ_{th} in a three-parameter Weibull model such as in Equation (8a) lacks a rationale. Hadid-Moud et al. [10] calibrated Equation (8a) with cleavage fracture data of steels A 508 and A533B, respectively. For A508 steel, shallow and sharp-notched round-notched bars (RNB) were tested at 153 and 123 K; while for A533B steel, single edge notched bend, SEM(B), specimens were tested at 103 K. Table 1 summarises the calibrated parameter values in [10] that provided the best agreement. As noted in [10],

> The four Weibull parameters in the distribution function are inter-dependent and thus one has to be pre-selected for the calibration process. Unlike the analysis for the pre-cracked data, V_0, was arbitrarily fixed to be 0.001 mm^3 while m was considered a free parameter.

As a result, for these notched specimens, A508 steel exhibits not only temperature dependence of threshold stress σ_{th} and the scale parameter σ_0 instead of a fixed value as presumed although the value of m remains unchanged (m = 23, 24) but also constraint (notch sharpness) dependence of all the three parameters (m, σ_{th} σ_0).

(3) *Involving both the plastic strain (ε_p) effect and a fixed-value threshold stress (σ_{th}).* A simple example is the combination of Equation (8a) with Equation (7) in [11]. Since both Equations (8a) and (7) are empirical expressions, the drawbacks associated with each of them are inherited by their resultant combination.

As a result of these efforts, the calibrated m does not change with temperature, while σ_0, and σ_{th} are temperature dependent [10–12]. Moattari et al. [16] described the effect of temperature on σ_0 as the sum of athermal and thermally activated stress contributions. In addition, the effect of geometrical constraint on the two model parameters has not been addressed. Overall, the dependence of temperature and specimen geometry on the model parameters (m and σ_0) is still in debate. This situation implies that the Beremin model and the modified models may suffer from some more fundamental physical imperfections, which necessitates a revisit to the formulation process of the Beremin model. Recently, a set of consecutive studies [1–3,17,19] have been pursued to understand the fundamental aspects of the stochastic cleavage fracture process. One of the critical conclusions is about the threshold stress (σ_{th}) for cleavage fracture. As interpreted in detail in [1,2,17], the precedence of plastic yielding over cleavage fracture determines the existence of a non-zero threshold stress (σ_{th}) higher than or at least equal to $\sigma_{1,0} = \eta\sigma_{ys} (\eta \geq 1)$, i.e. $\sigma_{th} \geq \sigma_{1,0} = \eta\sigma_{ys}$. Here, $\sigma_{1,0}$ is the maximum principal tensile stress (σ_1) on a volume element at the occurrence of its initial plastic yielding, σ_{ys} is the yielding stress, η is a coefficient. According to the von Mises yield criterion,

$$\left(\sigma_{1,0} - \sigma_2\right)^2 + \left(\sigma_2 - \sigma_3\right)^2 + \left(\sigma_3 - \sigma_{1,0}\right)^2 = 2\sigma_{ys}^2. \tag{13}$$

where σ_2 and σ_3 are the other two principal stresses. Moreover, $\sigma_{th} = \sigma_{1,0} = \eta\sigma_{ys}$ has been justified in [14–16], indicating that the threshold stress (σ_{th}) for cleavage fracture varies with temperature and strain rate (via σ_{ys}) and geometrical constraint or stress state (via η), instead of being a fixed value. To emphasise this very critical point of a non-fixed-value threshold cleavage stress (σ_{th}), consider three volume elements A, B, and C, each of which contains a microcrack with $\boldsymbol{n}$ being its normal to the microcrack surface. The volume element A is subjected to uniaxial tension, while B and C are in triaxial tension. However, C has a more severe stress triaxiality than B. These three different volume elements can be taken as the representative points in a smooth, a notched or a cracked specimen subjected to uniaxial tension, respectively, as shown in Figure 1, or can resemble different points located within a same notched (or cracked) specimen in tension, as exemplified in Figure 2.

Figure 1 schematically illustrates the variation of $\sigma_{1,0} = \eta\sigma_{ys}$with temperature for the three different volume elements. Note that $\eta_C > \eta_B > \eta_A = 1$. T_{A0}, T_{B0}, and T_{C0} denote the highest temperature for the occurrence of cleavage initiation in volume elements A, B and C in sequence. Now, let's assume that there would exist a fixed-value threshold cleavage stress $\sigma_{th} = Const$ independent of temperature and stress triaxiality (geometrical constraint), as represented by the orange solid horizontal line. At an arbitrary temperature T_x, due to the maximum principal tensile stress criterion, when $\sigma_1 \geq \sigma_{th}$, cleavage fracture should occur in all the three volume elements A, B and C. However, since there is $\sigma_{1,0,A}(T_X) < \sigma_{1,0,B}(T_X)$

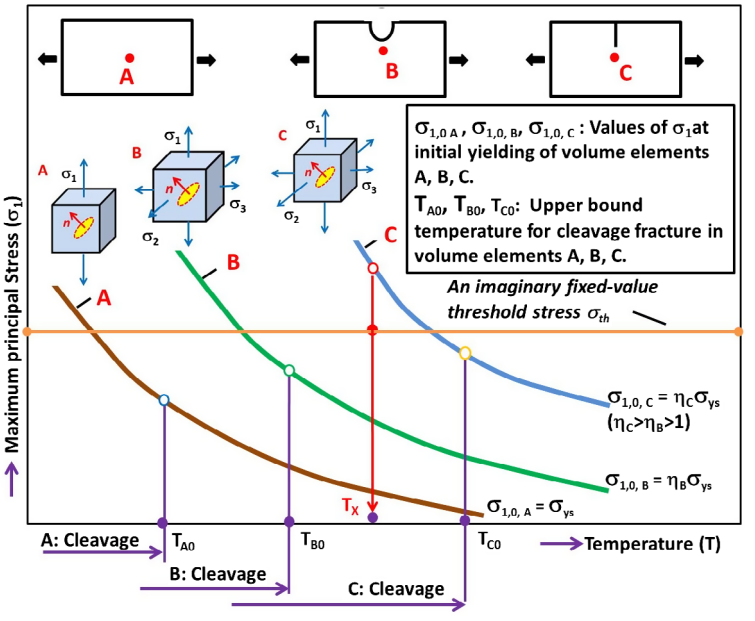

Figure 1. (Colour online) Schematic interpretation of the non-existence of a fixed-value threshold stress for cleavage fracture.

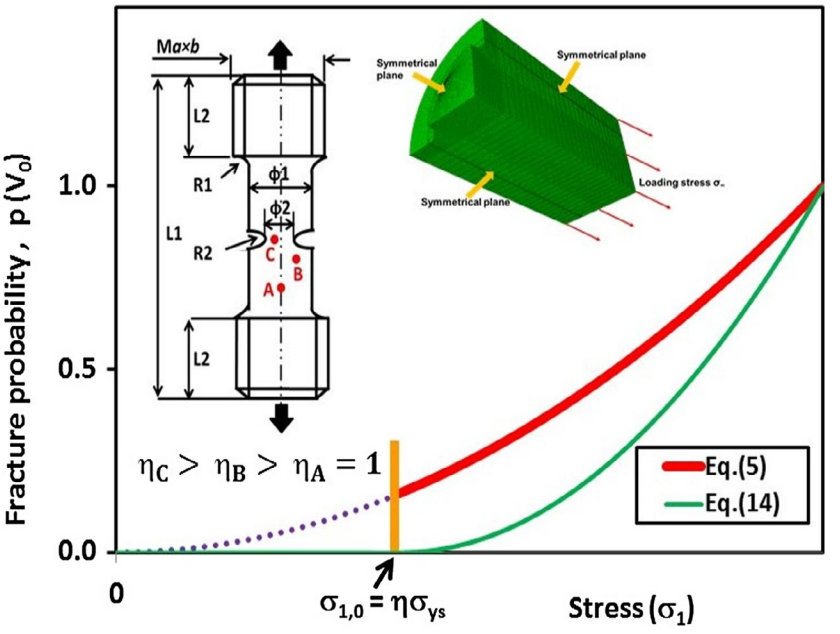

Figure 2. (Colour online) Schematic difference between Equation (5) for the Beremin model and the reformulated Equation (14).

$< \sigma_{th} < \sigma_{1,0,C}(T_X)$, it tells that for volume elements A and B, cleavage fracture does take place after the occurrence of plastic yielding, which is in accordance with the consensus of plastic yielding as a prerequisite condition to cleavage fracture; while for volume element C, it would suggest that cleavage fracture might occur prior to plastic yielding in the case of $\sigma_{th} < \sigma_1 < \sigma_{1,0,C}(T_X)$, which violates the basic consensus. In fact, due to the consensus, at $T = T_X$, only when $\sigma_1 \geq \sigma_{1,0,C}(T_X)$, can cleavage occur in volume element C. Furthermore, since there is $T_{A0} < T_{B0} < T_X$, cleavage fracture does not occur in volume elements A and B at $T = T_X$. One can try any other value of the threshold stress σ_{th} to test the sequential occurrence of plastic yielding and cleavage fracture in all the three volume elements. So long as σ_{th} is assigned a fixed value independent of temperature and stress state, the common physical understanding of cleavage fracture being preceded by plastic yielding is always violated. Since it is well established that at sufficiently low temperature, cleavage fracture stress equals to yielding stress in the case of uniaxial tension (volume element A in Figure 1), the relationship $\sigma_{th} = \sigma_{1,0} = \eta\sigma_{ys}$holds.

This finding has several direct consequences. First, since Equation (5) for the fracture probability of a volume element, $p(V_0)$, possesses the normalisation condition $0 \leq \sigma_1 \leq \sigma_0$ instead of $\eta\sigma_{ys} = \sigma_{th} \leq \sigma_1 \leq \sigma_0$. In theory, the adoption of Equation (5) implies that cleavage fracture can occur prior to plastic yielding ($0 \leq \sigma_1 \leq \sigma_{th} = \eta\sigma_{ys}$), which violates the basic physical mechanism of cleavage fracture preceded by plastic yielding. In practice, since the integral in Equation (1) or (2) is always confined within the plastic deformation zone, $\eta\sigma_{ys} \leq \sigma_1 \leq \sigma_0$is taken, so either $p(V_0)$ or the cumulative probability P never reaches zero, that is,

neither of them observes the normalisation condition as an axiom of probability. For the power-law size (a) distribution of plastic yielding induced micro-cracks in Equation (4), $p(V_0)$ is reformulated as below in [17]:

$$p(V_0) = (\sigma_1^m - \sigma_{1,0}^m)/\sigma_0^m, \quad \sigma_0 = \sqrt[m]{\sigma_u^m - \sigma_{1,0}^m} \tag{14}$$

where σ_u is a material constant. Equation (14) suggests that σ_0 varies with $\sigma_{1,0}$ (hence stress state and temperature dependent) instead of being a material constant as assumed by Beremin model. Figure 2 schematically highlights the difference between Equation (5) for the Beremin model and the reformulated Equation (14), in which a round notched tensile bar is embedded to show three points (A, B, and C) with different stress states and hence the value of $\sigma_{1,0}$. Also, the finite element (FE) model of one-eighth of the specimen to be used in this study is also embedded in Figure 2.

Second, the invalidity of Equation (5) and hence the Weibull stress definition Equation (2) inevitably refutes Equation (7) as its modification for the plastic strain (ε_p) correction. Third, Equation (8a) as the modified Weibull stress formulation via the introduction of a fixed-value threshold stress is disproved due to their inheritance of Equations (2) and (7).

The recognition of temperature and stress state dependence of cleavage threshold stress σ_{th} led to a reformulated statistical model for cleavage fracture in [2] and a proposed framework of statistical approaches to plastic yielding initiated cleavage fracture in [1]. Calibration of the reformulated statistical model with data generated from Monte Carlo simulation at individual volume element scale yielded temperature and stress state independent values of both statistical properties (m and σ_0) in [2]. This motivates us to apply the reformulated statistical model to investigate the effect of temperature on the two model parameters (m and σ_0) with experimental data from realistic notched or cracked specimens.

This work will proceed in the following sequence: (1). A brief introduction to the reformulated LA model; (2). An interpretation of the physical consistency of the new LA model to the principles of LA methodology with a summary of its differences with major existing LA models; (3). A summary of experimental data-set from a third party; (4). A detailed scheme for FE analysis and model calibration; (5). Result and analysis, followed by conclusions.

2. A brief to a new statistical model for cleavage fracture

In [1,20], it was proven in detail that Equation (3) as the basic weakest link formulation for the cumulative probability of brittle fracture is inaccurate. Therefore, the following model for the weakest link postulate based cumulative failure probability was proposed under the assumption of a uniform spatial distribution of microcracks:

$$P = 1 - exp\left\{ \int_{V_{pl}} ln\left[1 - p\left(V_0\right)\right] \cdot \frac{\mathrm{d}V}{V_0} \right\} \tag{15}$$

Under the maximum tensile stress (σ_1) fracture criterion, $\sigma_1 \geq S$, with S being the critical cleavage fracture stress for a given microcrack size a, $p\left(V_0\right)$ in Equation (15) is determined by

$$p\left(V_0\right) = \int_{a_c(\sigma_1)}^{a_{max}(\sigma_{1,0})} f(a)da = \int_{\sigma_{1,0}}^{\sigma_1} g(S)\mathrm{d}S \tag{16}$$

where $f(a)$ and $g(S)$ are the probability density function (PDF) of microcracks with respect to microcrack size (a) and the critical fracture strength (S), respectively.

In principle, Equation (16) and hence Equation (15) are applicable to any given expression of $f(a)$ or $g(S)$ for statistical microcrack distribution, so long as it physically exists. In total, nine (9) different PDFs of microcracks were evaluated to deduct the corresponding analytical solutions for $p\left(V_0\right)$ in [1]. The resultant mathematical expressions of the cumulative probability P possess different levels of complexity, which will in turn have specific impacts on the model calibration. As examples, when the PDF of microcracks is described by the power law of size distribution in Equation (4), the combination of Equations (14) and (15) leads to

$$P = 1 - \exp\left[\int_{V_{pl}} ln\left(\frac{\sigma_u^m - \sigma_1^m}{\sigma_u^m - \sigma_{1,0}^m} \right) \cdot \frac{\mathrm{d}V}{V_0} \right] \tag{17}$$

When the PDF of microcracks is described by the Weibull distribution of microscopic strength (S),

$$g(S) = m \cdot [(S - \sigma_{th})^{m-1}/\sigma_0^m] \cdot \exp[-(S - \sigma_{th})^m/\sigma_0^m] \tag{18}$$

where m and σ_0 are material constants,

$$p\left(V_0\right) = 1 - \exp\left[-\left(\frac{\sigma_1 - \sigma_{th}}{\sigma_0} \right)^m \right] \tag{19}$$

$$p = 1 - \exp\left[-\int_{V_{pl}} \left(\frac{\sigma_1 - \sigma_{1,0}}{\sigma_0} \right)^m \frac{\mathrm{d}V}{V_0} \right] = 1 - \exp\left[-\left(\sigma_W/\sigma_0\right)^m \right] \tag{20}$$

$$\text{with } \sigma_W = \left[\int_{V_{pl}} (\sigma_1 - \sigma_{1,0})^m \cdot \mathrm{d}V/V_0 \right]^{1/m} \tag{21}$$

Equation (21) is the redefined Weibull stress σ_W in analogy with Equation (2). It allows to take advantage of the well-developed calibration procedure for the following two-parameter Weibull statistics to calibrate Equation (20):

$$LnLn\left[1/(1-P)\right] = mLn\left(\sigma_W\right) - mLn\left(\sigma_0\right) \tag{22}$$

In comparison, a more complex procedure will be needed to calibrate Equation (17) owing to the existence of the stress state dependent quantity $\sigma_{1,0}^m$ in the denominator.

Equation (20) strictly adheres to plastic yielding as a prerequisite for cleavage fracture. Therefore, it is expected to be able to overcome the ambiguous calibration of the two Weibull parameters due to their temperature and constraint dependence. This work will adopt Equation (20) for studying the effect of temperature on the two model parameters m and σ_0. Before that, it is beneficial to summarise the consistency of the micromechanics based models and the major differences between the new model adopted in this study and the models proposed by other authors within the framework of LA methodology.

3. The consistency of micromechanics based LA models and the merits of the new model

A detailed critical review of existing micromechanics based LA models and a thorough description of the new model was given in [1]. The consistency of the micromechanics based LA models and the difference of the new model with the existing ones are closely interrelated.

3.1. The consistency of the micromechanics based statistical models

The reader is cautioned to clarify the differences between the following two aspects on the micromechanics based LA models:

(1) The physical consistency or justification of the methodology or principles of micromechanics based LA concept for cleavage fracture of steels;
(2) The adherence or consistency of a specific existing statistical model, e.g. in [7,10–12], to the methodology or principles of the micromechanics based LA concept.

The clarification of these two aspects is necessary. On one hand, if the micromechanics based LA methodology for cleavage fracture of steels is physically inconsistent or unjustifiable, LA would be conceptually wrong; while on the other hand, if some existing LA models violate the LA methodology or principles, these specific models are not in the position to invalidate the generic LA concept.

At a high level, physically, it is a consensus that cleavage fracture of steels is partitioned to two phases namely, microcrack formation and unstable microcrack

propagation. Moreover, microcrack formation can only occur in a plastically deformed volume element, that is, it is impossible for cleavage microcrack formation in an elastic volume element. The unstable microcrack propagation is commonly accepted to follow a stress based microscopic fracture criterion $\sigma_{eq} \geq S$ (σ_{eq} as the equivalent stress), with the maximum principal tensile stress criterion ($\sigma_{eq} = \sigma_1 \geq S$) being most commonly adopted. Mathematically, the weakest-link theory has been most widely adopted to describe the cleavage fracture event. Besides, one natural constraint, which is often neglected, is that the formulated statistical models must obey the basic mathematical rules. For example, any probability model has to conform to the normative axiom so that $P = 0$ corresponds to the nonoccurrence of fracture and $P = 1$ to the occurrence of fracture. As interpreted in detail in [2,17], one of the critical defects in the Beremin model is that it concludes that the probability for nonoccurrence of cleavage fracture is $P > 0$ due to the adoption of $\sigma_{th} = 0$, which violates the basic physical assumption of the precedence of plastic yielding over microcrack formation.

In a more detailed way, as stated in [1], for the sake of keeping its physical and mathematical consistency as well as the easiness of practical operation, the micromechanics based LA should at least fulfil the following principles:

(1) The weakest link theory applies;
(2) The random distribution of microcracks needs to be characterised in terms of the four attributes, namely, the spatial location, the orientation, the size and the shape of microcracks.
(3) The effect of spatial distribution of microcracks in ferritic steels on the cumulative failure probability needs to be addressed;
(4) The probability models are adaptable to any size/strength distribution of microcracks, instead of the power-law distribution only;
(5) Microcracks are mutually independent, so that the Griffith law is applicable to any individual microcrack;
(6) The occurrence of cleavage fracture is preceded by plastic deformation;
(7) The probability models conform to the normative axiom;
(8) Weibull statistics can be derived from the basic formulation of the cumulative failure probability;
(9) Model parameters can be calibrated/determined in different ways, including metallurgical, mechanistic and the hybrid methods.

Among these nine requirements, items (1), (5), (6), and (7) are self-evident; item (2) concerns how to explicitly formulate the fracture probability due to an individual microcrack; item (3) is a prerequisite to the mathematical formulation of the cumulative failure probability; item (4) determines the breadth of a LA model; item (8) is a testament to a LA model in that Weibull statistics itself is a weakest link model; item (9) ensures the practical feasibility of a LA model, which also implies that a LA model should be applicable to specimens with different geometries including pre-cracked ones and notched ones.

Conceptually, a LA model based on these principles will formulate the cumulative probability of failure (P) as a function of the volume (V_{pl}) of plastic yielding zone (as the fracture process zone) and the fracture probability ($p(a, V_0)$) of an elemental volume V_0 induced by an embedded microcrack under arbitrary loading as below,

$$P = F(p(a, V_0),\ V_{pl}) \tag{23}$$

Aside from these principles, the way to represent or formulate the fracture probability $p(a, V_0)$ of an elemental volume V_0 induced by an embedded microcrack calls for some practical treatment. Conceptually, $p(a, V_0)$ is the product of the probability $p_i(a, V_0)$ to form a microcrack in an elemental volume V_0 and the probability $p_p(a, V_0)$ for an existing microcrack of size a in the elemental volume V_0 to propagate unstably,

$$p(a, V_0) = p_i(a, V_0) \cdot p_p(a, V_0) \tag{24}$$

Moreover, by definition, $p_p(a, V_0)$ is expressed as

$$p_p(a, V_0) = \int_{\sigma_{th}}^{\sigma_{eq,max}} F(\sigma_{eq} \geq S) \cdot g(S) \cdot \mathrm{d}S \tag{25}$$

Substitution of Equation (25) in Equation (24) yields

$$p(a, V_0) = p_i(a, V_0) \cdot \int_{\sigma_{th}}^{\sigma_{eq,max}} F(\sigma_{eq} \geq S) \cdot g(S) \cdot \mathrm{d}S \tag{26}$$

where $\sigma_{eq,max}$ is the upper bound value of the equivalent stress σ_{eq}, $F(\sigma_{eq} \geq S)$ is the fracture probability of an existing microcrack, $g(S)$ is the PDF with respect to the fracture strength (S) of elemental volume V_0, $g(S) \cdot \mathrm{d}S$ is the probability of the existence of a microcrack with its strength between S and $S + \mathrm{d}S$, the product $F(\sigma_{eq} \geq S) \cdot g(S) \cdot \mathrm{d}S$ defines the probability that a microcrack with its strength in this range will cause fracture.

3.2. Further treatment of $p_i(a, V_0)$ and $p_p(a, V_0)$

At this point, further treatment of $p_i(a, V_0)$ and $p_p(a, V_0)$ is needed to build an executable statistical model. This necessitates an in-depth discussion of the physical interpretation of cleavage process. This work is based on the following most widely acknowledged consensus that the complete microscopic cleavage fracture process in a ferritic steel consists of three consecutive steps [1,13,21–28]:

- Step I. Nucleation of a microcrack at a defect, e.g. a second-phase brittle article, to form a particle-sized microcrack (Figure 3(a));
- Step II. Propagation of a microcrack across the boundary between the particle and the first matrix (ferrite) grain to form a ferrite grain-sized microcrack (Figure 3(b) and (c));
- Step III. Further propagation of the ferrite grain-sized microcrack across the grain boundary into contiguous grains (Figure 3(d)).

The essence is that cleavage fracture involves nucleation and propagation of a microcrack. This three-step process has been described in different ways with different terms. For example, Bordet et al. [25] stated that 'there are two distinct and necessary steps in order for cleavage fracture to take place: initiation and propagation'. In the propagation phase (steps II and III), an interface or grain boundary is a barrier for the microcrack to propagate. So the 'multiple barrier model' is alternatively used in the literature [13,26]. The terms 'nucleation', 'initiation', and 'formation' of a microcrack have been alternatively used in the literature to denote the formation of a *particle-sized* microcrack in step I. Now the following three aspects are critical to understand a statistical model:

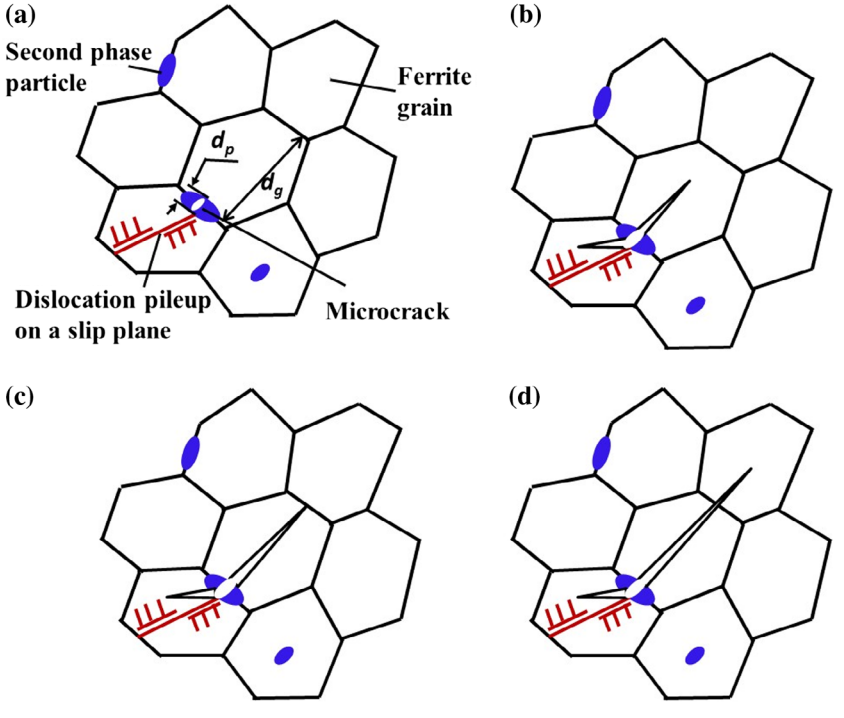

Figure 3. (Colour online) Schematic illustration of the three sequential phases in a cleavage fracture process: (a) Nucleation of a microcrack via breakage of a second-phase particle due to stress concentration ahead of a dislocation pileup; (b) Propagation of the second-phase particle-sized crack into the matrix ferrite grain; (c) Arrest of the ferrite grain-sized crack at ferrite/ferrite grain boundary; (d) Propagation of the ferrite grain-sized crack into neighbouring ferrite grains.

- Nucleation mechanisms of particle-sized microcracks;
- The critical event or controlling step in a cleavage fracture process;
- State of the art in mathematical treatment of the statistical contributions of microcrack nucleation and propagation.

3.2.1. Nucleation mechanisms of particle-sized microcracks

Numerous researches have been reported on the nucleation or initiation micromechanisms of microcracks in steels relating to cleavage fracture, such as in [22,24,29–39]. Echeverría-Zubiría et al. [32] summarised the rich variety of microcrack initiation mechanisms into three types as listed in Table 2. Two points were emphasised: (1). Microcrack initiation is strain controlled rather than stress controlled; (2). It is difficult to claim only one mechanism in effect for microcrack initiation and exclude other mechanisms. Both aspects need to be properly addressed in formulating $p_i(a, V_0)$ as the probability for microcrack formation. For example, Wang et al. [40] observed that in notched specimens of a C–Mn steel with the coexistence of (either fine or coarse) carbides and non-metallic inclusions MnS or complex oxides with Al, Mn, Fe, Ca and Ti, crack nucleation is induced by debonding or breakage of inclusions instead of carbides, but the controlling step for cleavage fracture is the propagation of a ferrite grain-sized crack into adjacent ferrite grains rather than the propagation of the inclusion particle-sized crack across the inclusion/ferrite interface, independent of the size and number of carbide particles. At 77 K, microcracks are nucleated at spherical inclusions ahead of notch root; while at 143 K, microcracks are nucleated at spherical inclusions ahead of the elongated larger string inclusions. He et al. [41] reported that at 77 K, microcracks initiate in the cementite lamellae rather than the MnS inclusions in a ferritic-pearlitic steel.

3.2.2. The critical event or controlling step in a cleavage fracture process

It is logically reasonable to assume that any of the three steps in a cleavage fracture process can be the controlling step or the critical event. As summarised by Chen

Table 2. Three types of microcrack initiation mechanisms [32].

Microcrack nucleation mechanism	Related microstructural features	
	Microstructural attributes	Examples
Breakage/cracking of a brittle phase	Brittle particle	Carbides; non-metallic inclusions, e.g. MnS, TiC, (Ti, N)(Ti,N,Ca, Al, Mg, Mn, O)
	Hard second phase	Martensite–Austenite (M–A) constituent; Pearlite colony
Debonding of a brittle phase from matrix	Brittle particle	MnS
	Hard second phase	M–A constituent
Voids	Close to or at notch root, without presence of carbides or inclusions	Microvoids
	A brittle phase in between ductile voids	MnS inclusion or M–A constituent between ductile voids

et al. [24], each of the three steps has once been proposed as the critical event: In the early 1950s, the nucleation of a particle-sized microcrack (step I in the three-step cleavage fracture process) was believed to be the most difficult step, with the role of dislocation pileup being emphasised; in the early 1960s, the propagation of a ferrite grain-sized microcrack was accepted as the critical event (step III in the three-step cleavage fracture process), with the matrix grain size being recognised as the dominant microstructural dimension; from the late 1960s to 1980s, the propagation of a carbide or other second-phase particle-sized microcrack across the brittle particle-to-ferrite grain interface into the matrix was identified as the controlling step (step II in the three-step cleavage fracture process), with the particle size being identified as critical microstructural dimension. During this time, Oates and Griffiths [42] found that for a 3% silicon iron, the critical event changed from the propagation of a ferrite grain-sized microcrack (step III in the three-step cleavage fracture process) in a smooth tensile specimen to the propagation of a carbide particle-sized microcrack (step II in the three-step cleavage fracture process) in a notched specimen.

The changeability of controlling steps for cleavage fracture has been more broadly verified since the late 1980s. Such a change can result from the variation of temperature, stress state, and microstructures. Lin et al. [43] suggested the changes of controlling step from microcrack nucleation (step I in the three-step cleavage fracture process) to carbide particle-sized crack propagation (step II in the three-step cleavage fracture process) and then to ferrite grain-sized crack propagation (step III in the three-step cleavage fracture process) as temperature increases. Li and Yao [22,23] observed that in smooth tension of a low-carbon steel, below the ductile-to-brittle transition temperature (DBTT), at which the cleavage fracture stress reaches minimum, the critical event or controlling step is microcrack nucleation; while above the DBTT, cleavage fracture is controlled by the propagation of a ferrite grain-sized microcrack instead of a cracked carbide. He et al. [41] used smooth cylindrical tensile specimens, notched cylindrical tensile specimens, and side edge notched bending specimens to study the effect of stress state on the critical event of cleavage fracture in a ferrite-pearlitic steel. It was concluded that crack propagation is the critical event that controls cleavage fracture at low stress triaxiality and high Lode angle parameter; while crack initiation/nucleation is the controlling step at higher stress triaxiality and lower Lode angle parameter. Chen and colleagues [24,44] reported change of critical events of cleavage fracture of low-alloy steels from crack propagation to crack nucleation due to variations of grain size, carbon and impurity element contents, test temperature, loading rate, pre-strain, and stress triaxiality. Bose Filho et al. [36,37] compared cleavage fracture of ferritic welds in notched and fatigue pre-cracked specimens. In both types of specimens, the unstable propagation of microcracks initiated from breakage or debonding of inclusions is the controlling step for cleavage fracture. However, the sizes of inclusions to initiate cleavage fracture in pre-cracked specimens are much smaller than those in notched specimens. From statistical point of view,

this difference may imply different statistical distributions of microcracks in both types of specimens. These results together raised the attentions that the critical event observed in a notched specimen can be different from that observed in a cracked specimen, which is critical in establishing or evaluating a statistical model of cleavage fracture, particularly in the aspects of the treatment of $p_i\left(a, V_0\right)$ and $p_p\left(a, V_0\right)$ and the statistical distribution of microcracks.

Based on the work of [43,44], the change of controlling steps in a cleavage fracture process under different conditions can be interpreted as follows with both the driving force and the resistance to unstable cleavage fracture being synchronised. Take the idealised situation that the surface of an arbitrary microcrack is always normal to the local maximum tensile principal stress σ_1. Under the maximum tensile principal stress fracture criterion, one gets

$$\sigma_1 = Q\left(\sigma_{ys} + \Delta\sigma_{ys}\right) \geq S_p = \sqrt{\frac{\pi E \gamma_{p/g}}{2(1-\nu^2)d_p}} \tag{27}$$

for a particle-sized penny-shaped microcrack of diameter d_p and strength S_p to propagate the *p*article-to-matrix (ferrite) *g*rain (*p*/*g*) interface, and

$$\sigma_1 = Q\left(\sigma_{ys} + \Delta\sigma_{ys}\right) \geq S_g = \sqrt{\frac{\pi E \gamma_{g/g}}{2(1-\nu^2)d_g}} \tag{28}$$

for a matrix (ferrite) grain-sized penny-shaped microcrack of diameter d_g and strength S_g to propagate the first matrix (ferrite) *g*rain-to-matrix (ferrite) *g*rain (*g*/*g*) boundary.

Here $\gamma_{p/g}$ is effective surface energy or the critical strain energy release rate [43] for dynamic propagation through the *p*article-to-matrix (ferrite) *g*rain (*p*/*g*) interface into the matrix (ferrite) grain; $\gamma_{g/g}$ is effective surface energy or the dynamic critical strain energy release rate for propagation through the first matrix (ferrite) *g*rain-to-matrix (ferrite) *g*rain (*g*/*g*) interface. $\gamma_{g/g}$ can be further rewritten as $\gamma_{g/g} = \gamma_s + w_p$, where γ_s is the surface energy of ferrite, w_p is the plastic work done per unit area in propagating the microcrack [45]. Crack propagation into the ferrite (step III) is undoubtedly accompanied by plastic deformation, while the propagation of a particle-sized microcrack through the *particle-to-matrix (ferrite) grain* interface (step II) is expected to incur less severe plastic deformation at the interface. As a result, a more pronounced temperature dependence on $\gamma_{g/g}$ is expected than on $\gamma_{p/g}$ [43]. San Martin and Rodriguez-Ibabe [46] estimated that for a Ti-V microalloyed ferrite-pearlite steel, $\gamma_{p/g} = 7$ J/m^2 with no or slight change with temperature, while $\gamma_{g/g}$ are much higher with much stronger temperature dependence. Despite the same conclusion in [46] on the temperature dependence of $\gamma_{g/g}$ with the analysis in [43], the estimated values of $\gamma_{g/g}$ are very rough. Specifically, at 253 K, 14 estimated values of $\gamma_{g/g}$ were obtained, with the average value being 81.1 J/m^2, the minimum and the maximum being 23.7 and 188.5 J/m^2,

respectively; at 223 K, 12 estimated values of $\gamma_{g/g}$ were obtained, with the average value being 200.6 J/m^2, the minimum and the maximum being 29 and 481 J/m^2, respectively; at 203 K, only two values (58.1 and 44.9 J/m^2) were estimated to give an average of 51.5 J/m^2. While the average value of $\gamma_{g/g}$ at 223 K (200.6 J/m^2), is higher than at 203 K (58.1 J/m^2) by almost 150 J/m^2, it is unfavourably significantly higher than that at 253 K (81.1 J/m^2) by almost 120 J/m^2. The difference of $\gamma_{g/g}$ at 203 K and 253 K is only ~30 J/m^2.

According to Equations (27) and (28), there is

$$S_g = S_p \sqrt{\left(\frac{d_p}{d_g}\right)\left(\frac{\gamma_{g/g}}{\gamma_{p/g}}\right)} \tag{29}$$

Given that $d_p \ll d_g$ and the premise that $\gamma_{g/g}$ has a stronger temperature dependence than $\gamma_{p/g}$. At certain low temperature, $S_p > S_g$ is expected, so that the critical event is the propagation of a particle-sized microcrack across the particle/ferrite grain boundary (step II); while at higher temperatures, the anticipated rapid increase of $\gamma_{g/g}$ will lead to $S_p < S_g$, so that the critical event is the propagation of a ferrite grain-sized microcrack across the first ferrite/ferrite grain boundary (step III). Evidently, the temperature dependence of effective surface energy supports microcrack propagation as the controlling step for cleavage fracture, whether it is via step II or step III.

The above discussion is based on the existence of a nucleated microcrack, which is influenced by plastic strain. Adding the driving force $\sigma_1 = Q(\sigma_{ys} + \Delta\sigma_{ys})$ into consideration, the change of critical event, which may be either from nucleation controlled (step I) to propagation controlled mechanism (step II or III), or from propagation of a particle-sized microcrack (step II) to propagation of a ferrite grain-sized microcrack (step III), with stress state, loading rate, pre-strain and other conditions can be interpreted [44].

3.2.3. Mathematical treatments of the contributions of microcrack nucleation and propagation

Physically, it is well accepted that both the nucleation and propagation of a microcrack are stochastic processes. The contributions of microcrack nucleation and propagation are treated in three different ways in various statistical models for cleavage fracture:

- Approach I: Microcrack nucleation as the controlling step. $p_p(a, V_0) = 1$, $p(a, V_0) = p_i(a, V_0)$. For example, one of the Prometry models [47] describes the strength or resistance of microcrack nucleation with the three-parameter Weibull statistics, while microcrack propagation is certain.
- Approach II: Microcrack propagation as the controlling step. $p_i(a, V_0) = 1$, $p(a, V_0) = p_p(a, V_0)$. A majority of existing statistical models fall into this category, including the Beremin model [7,13] and the model used in this

study [1,2]. As stated by Bordet et al. [25], no distinction is made whether the critical event is the propagation of particle-sized microcracks into the matrix phase (step II of cleavage fracture process) or that of ferrite grain-sized microcracks into neighbouring grains (step III of cleavage fracture process). If there is a change of the controlling step from step II to step III or vice versa at different temperatures, it will be reflected in the change of calibrated model parameters.

- Approach III: Microcrack propagation as the controlling step but with a quantified contribution of microcrack nucleation. $p_i(a, V_0) \neq 1$, $p_p(a, V_0) \neq 1$. A second Prometry model [47] expresses the strength of microcrack nucleation in a three-parameter Weibull format and that of microcrack propagation in a two-parameter Weibull format. Besides, Bordet et al. [25] and Shibanuma et al. [48] also proposed their expressions for the probability of microcrack formation $p_i(a, V_0)$, while the term $p_p(a, V_0)$ is addressed in different ways. The accuracy of this approach largely depends on how pertinently to quantify the coexisting multiple mechanisms of microcrack nucleation as shown in Table 2.

For either approach II or III, certain approximate treatment on formulating the probability $p_p(a, V_0)$ for unstable propagation of an existing microcrack is also needed. By definition, $p_p(a, V_0)$ is affected by not only the statistical distribution of microcracks in terms of their size, shape and orientation, but also the stress based microscopic fracture criterion to be adopted. In reality, a circular, penny shaped microcrack is only an idealised geometrical model of microcracks. Depending on the specific phase of material constituent to be broken to form a microcrack, the exact geometry of a microcrack can be far from a penny shaped model. Then a shape factor η should be introduced to the Griffith law $S = \sqrt{\eta E\gamma/(1-\nu^2)a}$ to represent the microscopic cleavage fracture resistance S as a function of the characteristic size a and the shape factor η, and the effective surface energy γ. However, the statistical distribution of the shape factor η remains unknown. So the practical treatment is either to directly assume $g(S)$ as the PDF with respect to the fracture strength (S) of elemental volume V_0 regardless of specific shapes of microcracks, or to assume all microcracks to be penny shaped with a size distribution $f(a)$, as Equation (4) in the Beremin model. Furthermore, the formulation of $F(\sigma_{eq} \geq S)$ in Equation (25) depends heavily on the microcrack orientation and exact stress state in consideration. The surface of an arbitrary microcrack in a volume element V_0 does not necessarily always take the orientation perpendicular to the maximum principal tensile stress σ_1 so as to satisfy the maximum tensile principal stress σ_1 based microscopic fracture criterion $\sigma_1 \geq S$. The normal tensile stress component σ_n based microscopic fracture criterion $\sigma_{eq} = \sigma_n \geq S$ seems more appropriate than $\sigma_1 \geq S$ to reflect the effect of microcrack orientation. In [49], the analytical solution to the fracture probability $F(\sigma_{eq} = \sigma_n \geq S)$ induced by

a randomly oriented microcrack under multi-axial loading for the normal tensile stress criterion $\sigma_{eq} = \sigma_n \geq S$ is formulated as follows:

$$F(\sigma_n \geq S) = \begin{cases} 0 & (S > \sigma_1 \geq \sigma_2 \geq \sigma_3) \\ 1 - \frac{2}{\pi}\int_0^{\frac{\pi}{2}} \sqrt{\Phi_1(S)}d\beta & (\sigma_1 \geq S > \sigma_2 \geq \sigma_3) \\ 1 - \frac{2}{\pi}\int_{arccos\sqrt{\Psi_1(S)}}^{\frac{\pi}{2}} \sqrt{\Phi_1(S)}d\beta & (\sigma_1 \geq \sigma_2 \geq S > \sigma_3) \\ 1 & (\sigma_1 \geq \sigma_2 \geq \sigma_3 \geq S) \end{cases} \quad (30a,b,c,d)$$

with

$$\Phi_1(S) = \frac{(S - \sigma_3) - (\sigma_2 - \sigma_3)cos^2\beta}{(\sigma_1 - \sigma_3) - (\sigma_2 - \sigma_3)cos^2\beta} \quad (31)$$

$$\Psi_1(S) = \frac{S - \sigma_3}{\sigma_2 - \sigma_3} \quad (32)$$

where σ_1, σ_2, and σ_3 are the principal stresses acting on the volume element V_0 embedded with a microcrack, $\sigma_n = \sigma_3 + (\sigma_1 - \sigma_3) \cdot cos^2\alpha + (\sigma_2 - \sigma_3) \cdot cos^2\beta \cdot sin^2\alpha$, α and β are the angles to the normal vector of the microcrack surface from σ_1 and from σ_2 in the plane perpendicular to the direction of σ_1, respectively.

One would argue that some other multi-axial stress based microscopic fracture criterion $\sigma_{eq} \geq S$, such as those listed in the Appendix A of [2], might be more appropriate than $\sigma_{eq} = \sigma_n \geq S$ or $\sigma_{eq} = \sigma_1 \geq S$. But the analytical solution to $F(\sigma_{eq} \geq S)$ for such a fracture criterion might be more complicated than that to $F(\sigma_n \geq S)$ in Equations (30a,b,c,d) or even unavailable. Again, for simplicity, in most cases, the maximum tensile principal stress criterion $\sigma_{eq} = \sigma_1 \geq S$ is adopted, which lead to

$$F(\sigma_1 \geq S) = \begin{cases} 1 & (\sigma_1 > 0) \\ 0 & (\sigma_1 \leq 0) \end{cases} \quad (33)$$

In turn, Equation (25) reduces to the simplest format:

$$p_p(a, V_0) = \int_{\sigma_{th}}^{\sigma_1} g(S) \cdot dS \equiv \int_{a(\sigma_1)}^{a(\sigma_{th})} f(a)da \quad (34)$$

According to the theorem of PDF of a function with a continuous random variable, *f(a)* and *g(S)* are transferrable to each other:

$$g(S) = \left|\frac{\partial a}{\partial S}\right| f(a) = \frac{2k^2}{S^3} f\left(\frac{k^2}{S^2}\right) \quad (35)$$

$$f(a) = \left|\frac{\partial S}{\partial a}\right| g(S) = \frac{k}{2a\sqrt{a}} g\left(\frac{k}{\sqrt{a}}\right) \tag{36}$$

where $k = \sqrt{\eta E\gamma/\left(1-\nu^2\right)}$ according to the Griffith law.
The adoption of the simplest maximum tensile principal stress criterion $\sigma_{eq} = \sigma_1 \geq S$ allows to rewrite Equation (26) as follows:

$$p\left(a, V_0\right) = p_i\left(a, V_0\right) \cdot \int_{\sigma_{th}}^{\sigma_1} g(S) \cdot \mathrm{d}S \equiv p_i\left(a, V_0\right) \cdot \int_{a(\sigma_1)}^{a(\sigma_{th})} f(a)da \tag{37}$$

$$\text{and } p_i\left(a, V_0\right) = 1, \quad p\left(a, V_0\right) = \int_{\sigma_{th}}^{\sigma_1} g(S) \cdot \mathrm{d}S \equiv \int_{a(\sigma_1)}^{a(\sigma_{th})} f(a)da \tag{38}$$

The discussions above in this section interpret the complexity in strictly formulating the fracture probability ($p(a, V_0)$) of an elemental volume V_0 induced by an embedded microcrack as given in Equation (26) and the exemplified necessary approximate treatments as given in Equations (37) and (38). Whether Equation (37) is more accurate than Equation (38) or not will largely depend on how accurately to formulate $p_i(a, V_0)$. For either of these two equations, there has been already adopted a series of approximations from the shape and orientation of microcracks to the microscopic fracture criterion $\sigma_{eq} \geq S$. However, compared to the nine principles for the micromechanics based LA, these approximate treatments are secondary factors and do not hurt the physical consistency of LA methodology.

Adding to the complexity of the microscopic cleavage fracture process, the common acceptance of microcrack nucleation as a plastic strain controlled event inevitably suggests a non-uniform spatial (volumetric) distribution of microcracks within a volume of non-uniform plastic deformation such as in a notched or cracked specimen, even if the second-phase particles take a uniform spatial distribution. The number of microcracks nucleated in a plastic volume element close to a notch/crack tip is expected to be larger than that in an equal-sized plastic volume element far away from the notch/crack tip. So far, all the existing models including the one being considered in this study either adopt a Poisson or uniform law for the spatial distribution of microcracks to set up the basic formulation for the cumulative fracture probability P, e.g. Equations (3) and (15). Theoretically, the basic formulation for the cumulative fracture probability P in accordance with a non-Poisson, non-uniform spatial distribution of microcracks is clearly a missing point. This is a rather more difficult topic than how to properly quantify $p_i\left(a, V_0\right)$ and $p_p\left(a, V_0\right)$for more delicate representation of the fracture probability of an element volume (V_0), $p\left(a, V_0\right)$, since it demands more detailed understanding and characterisation of the mechanisms and spatial distribution

of microcrack nucleation. Similar to the existing practice of adopting the maximum tensile principal stress fracture criterion $\sigma_1 \geq S$ instead of the more complex multi-axial equivalent stress fracture criterion $\sigma_{eq} \geq S$, the uniform spatial distribution assumption is employed while we are exploring a proper representation of the cumulative fracture probability P for a bulk volume V for a non-Poisson, non-uniform spatial distribution of microcracks. As an initial effort, recently, a generalised weakest-link statistical model for the strength of quasi-brittle materials was proposed to account for a uniform, or a non-Poisson, non-uniform spatial distribution of microcracks [50].

To sum up, so long as the afore cited nine principles are observed, the physical consistency of micromechanics based LA methodology is assured. However, the existing LA models more or less violate some of these nine principles. This motivated the proposal of a new LA model in [1,2]. For example, the Beremin model conceptually abides by the weakest link theory, but the basic formulation Equation (3) for cumulative probability is mathematically incorrect. As a consequence, Weibull statistics cannot be derived from the basic formulation Equation (3). The Beremin model claims to accept the physical assumption that plastic yielding precedes microcrack formation, but the resultant formulation for the fracture probability ($p(a, V_0)$) of an elemental volume V_0 induced by an embedded microcrack in Equation (5) refutes this physical assumption, which also causes the nonconformity of the probability model in Equation (1) to the normative axiom. Besides, the model is only limited to the power-law distribution of microcrack size. In comparison, the new LA introduced in Section 2 fulfils all the nine principles. Since the new LA is applicable to any size/strength distribution of microcracks, including but not limited to the power-law distribution of microcrack size, we now compare the major differences of the Beremin model and the new LA model in Table 3 under the five exactly same physical assumptions set by Beremin model.

As shown in Table 3, the five basic assumptions in the Beremin model are all reasonable and pertinent to the physical understanding of cleavage fracture. The fundamental defects lie in the false mathematical formulations of the cumulative probability $P(V)$ and the fracture probability of a volume element $p(\sigma, V_0)$. In other words, the resultant mathematical formulations are not consistent to the physically sound assumptions. This tells two things: First, the contribution of the Beremin model in pioneering the original concept of the LA methodology should be highly acknowledged; second, correct mathematical formulations must be in place to substantiate the LA methodology.

In comparison, many of the other LA models are far inferior to the Beremin model in terms of the adherence to the basic physical assumptions. Some of them might be more properly categorised as empirical models. For example, one cannot tell what the basic formulation of the cumulative probability (to the level of Equation (3) or (15)) and the exact assumption for microcrack distribution $f(a)$ or $g(S)$ are for the two statistical models represented by Equations (8b) and (9). The

Table 3. The Beremin model versus the new LA model under the five assumptions for the Beremin model.

Model assumptions & attributes	Beremin model	New LA model
Model assumption #1	Uniform spatial distribution of microcracks	
Model assumption #2	Weakest-link model	
Basic formulation of cumulative probability P(V)	Equation (3): $P(V) = 1 - \exp\left[-\int_V p(\sigma, V_0)\frac{V}{V_0}\right]$	Equation (15): $P(V) = 1 - \exp\left\{\int_V \ln\left[1 - p(\sigma, V_0)\right]\frac{V}{V_0}\right\}$
Self-consistency check	$V = V_0$: Equation (3) $\Rightarrow\ P\left(V_0\right) = 1 - \exp\left[-p(\sigma, V_0)\right]$ *False!*	$V = V_0$: Equation (15) $\Rightarrow\ P\left(V_0\right) = p(\sigma, V_0)$ *True!*
Model assumption #3	Plastic yielding as a prerequisite for cleavage fracture $\Rightarrow$ Initial yielding as the threshold stress state for cleavage fracture	
Model assumption #4	Microscopic fracture criterion : $\sigma = \sigma_1 \geq S$	
Model assumption #5	Power-law distribution of microcrack size, Equation (4): $f(a) = \mu \cdot a^{-\kappa}$, $m = 2\kappa - 2$	
Fracture probability of a volume element V_0, $p(\sigma,V_0)$	Equation (5): $p\left(\sigma, V_0\right) = \left(\frac{\sigma_1}{\sigma_0}\right)^m$	Equation (14): $p\left(\sigma, V_0\right) = \frac{\sigma_1^m - \sigma_{1,0}^m}{\sigma_u^m - \sigma_{1,0}^m}$
Cumulative probability	Equation (1): $P(V) = 1 - \exp\left[-\int_{V_{pl}}\left(\frac{\sigma_1}{\sigma_0}\right)^m \frac{V}{V_0}\right]$	Equation (17): $P(V) = 1 - \exp\left[\int_{V_{pl}} Ln\left(\frac{\sigma_u^m - \sigma_1^m}{\sigma_u^m - \sigma_{1,0}^m}\right)\frac{V}{V_0}\right]$
Model applicable range	$0 \neq \left(\frac{\sigma_{ys}}{\sigma_0}\right)^m \leq p\left(\sigma, V_0\right) \leq 1 \Rightarrow \sigma_{ys} \leq \sigma_1 \leq \sigma_0$	$0 \leq p\left(\sigma, V_0\right) \leq 1 \Rightarrow \sigma_{1,0} \leq \sigma_1 \leq \sigma_u$
Assessment of cumulative probability	*Violate normality axiom of probability.* $0 \neq P_{min} \leq P(V) \leq 1 - \exp(-V/V_0) \neq 1$ *Violate normality axiom of probability*	$0 \leq P(V) \leq 1$

Beremin model has been used for notched and cracked specimens, but Equations (8b) and (9) are confined to cracked specimens.

3.3. The differences between the new model and other models

Based on the discussions in Sections 1, 2, 3.1, and 3.2, and more detailed explanations in [1,2], the differences between the new LA model in Section 2 and the previous models can be highlighted as follows:

(1) The new model is consistent to the nine principles for the LA methodology, while the existing models violate some critical principles. Among the existing models, the Beremin model is more superior to others in terms of the physical assumptions, despite its defective mathematical formulations.

(2) One major merit of the new LA model is that it establishes the basic formulation for the weakest-link statistics in Equation (15) to replace the defective expression Equation (3) used by the Beremin model. Thus, it ensures the model to conform to the *normality axiom of probability,* which is a starting point for any probability model.

(3) The second merit of the new LA model is that it proposes to adopt the initial yielding stress state of a volume element to depict the threshold stress state for a volume element to incur cleavage fracture. Although at the initial yielding state, the von Mises equivalent stress $\sigma_{VM} = \sqrt{\left[\left(\sigma_1 - \sigma_2\right)^2 + \left(\sigma_2 - \sigma_3\right)^2 + \left(\sigma_3 - \sigma_1\right)^2\right]/2}$ always equals to the yield stress σ_{ys}, the corresponding effective stress σ_{eq} for cleavage fracture ($\sigma_{eq} \geq S$) at initial yielding is a function of yield stress σ_{ys} and stress state or constraint. For example, in the case of the maximum tensile principal stress criterion $\sigma_{eq} = \sigma_1 \geq S$, the corresponding value of σ_1 is denoted as $\sigma_{1,0}$ and $\sigma_{1,0} = \eta\sigma_{ys}(\eta \geq 1)$, which satisfies Equation (13) for the von Mises yield criterion. This ensures that physically, every volume element in an arbitrary specimen, either with or without a notch or a crack, always satisfies the basic assumption of cleavage fracture preceded by plastic yielding; while mathematically, the probability model is self-consistent. In contrast, a fixed-value threshold such as in Equation (8a) will violate the basic assumption of cleavage fracture preceded by plastic yielding; the $\sigma_{W,min}$ based models would be not applicable to specimens without a pre-crack, in addition to other demerits discussed above.

(4) The new LA model reasonably derives three-parameter Weibull statistics while other models cannot.

4. Experimental fracture data-set

For the purpose to study the effect of temperature on m and σ_0, it is advantageous to use experimental fracture data-sets already generated and published by a third-party, particularly if they have been used to calibrate other statistical models. This allows us to make cross comparisons between different statistical models. Moreover, based on the previous studies [40,44,51–53], cleavage fracture in a notched specimen is microcrack propagation controlled (either step II or step III) unless at very low temperatures, this work chose to use fracture data of notched specimens to check on the model. Should there be a change in the critical event within the temperature range of concern, a corresponding change in the calibrated model parameters is expected. For the case of cracked specimens to be evaluated in the next phase of work, the critical event can be much different between a notched specimen and a cracked specimen.

In [51–53],researchers at India's Bhabha Atomic Research Center published cleavage fracture stress data of a ferritic low alloy steel 20MnMoNi55 commonly used for RPV construction obtained from testing circumferentially notched round tensile specimens at four subzero temperatures (123, 173, 203, and 223 K). In [53], cleavage fracture stress data of another nuclear grade carbon steel SA333 (Grade 6) were also reported on circumferentially notched round tensile specimens at two subzero temperatures (123, 173 K). The material properties of both steels relevant to the current study are summarised in Table 4. The chemical composition of 20MnMoNi55 is (in weight-%): C-0.21, Si-0.21, Mn-1.3, P-0.009, S-0.001, Ni-0.68, Cr-0.05, Mo-0.494, V-0.01, Al-0.029, Fe-balance. The chemical composition of SA333 (Grade 6) is (in weight-%): C-0.14, Si-0.25, Mn-0.90, P-0.016, S-0.018, Ni-0.25, Cr-0.05, Fe-balance. The microstructure of 20MnMoNi55 consists of ferrite-carbide aggregate, with carbide particles distributed within ferrite and also at prior austenite grain boundaries, while SA333 steel has banded ferrite-pearlite structure. The true stress-plastic strain curves of 20MnMoNi55 at the four temperatures reported in [23,24] are used as input to FE analysis, which are given in Figure 4.

Refer to the geometric sketch of specimen embedded in Figure 2, the specimen dimensions in millimetre are $L_1 = 76, Ma \times b = M20 \times 1.5, L_2 = 20, \emptyset_1 = 14, \emptyset_2 = 7.7, R_1 = 4, R_2 = 1.25$.

Table 4. Material properties of low alloy ferritic steels 20MnMoNi55 and SA333 (Grade 6).

Steel	20MnMoNi55	SA333 (Grade 6)
Young's modulus of elasticity E (GPa)	210 [51], 200 [52]	/
Poisson's ratio v	0.3 [51,52]	/
Temperature (K)	Yield strength σ_{ys} (MPa)	
223	537[52]; 542 [53]	/
203	558 [51]; 576 [53];	/
173	609 [51]; 600[52]; 597 [53]	518 [53]
123	685 [52]; 674 [53]	559 [53]

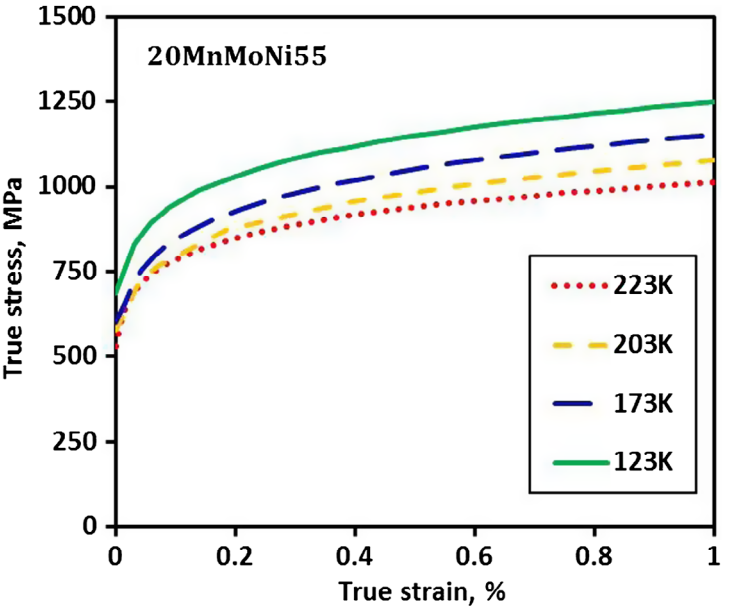

Figure 4. (Colour online) True stress-plastic strain curves of 20MnMoNi55 for finite element analysis [51,52].

At each of the four temperatures, thirty specimens were tested. Hence, a total number of 120 tests were done. The nominal fracture strength σ_N is converted from the measured fracture load F and the net section area at the notch according to $\sigma_N = 4F/(\pi\emptyset_2^2)$. The measured σ_N data-set is summarised in the Weibull distribution plot in Figure 5. The cumulative probability of failure P in the axis of ordinates for each strength datum is calculated according to $P(\sigma_{N,i}) = (i - 0.3)/(N + 0.4)$, where $N = 30$, $i = 1, 2, \ldots N$, $P(\sigma_{N,i})$ is the rank probability for the ith strength value $\sigma_{N,i}$ when all the thirty strength data points at each temperature are arranged in an ascending order. Ten out of thirty data points are circled at 123 and 223 K, respectively, which are used in FE calculation for model calibration. In [52], the Beremin model was calibrated according to Equations (1) and (22) by performing FE analysis for all 30 fracture strength data at each of the three temperatures namely, 123, 173, and 223 K, respectively. The calibration results are summarised in Table 5. In [53], the two-parameter Weibull distribution was directly applied to the nominal fracture strength σ_N as below:

$$P = 1 - \exp\left[-\left(\frac{\sigma_N}{\sigma_0}\right)^m\right] \tag{39}$$

Linear regression (LR) method was adopted to determine the two Weibull parameters (m and σ_0), as also summarised in Table 5.

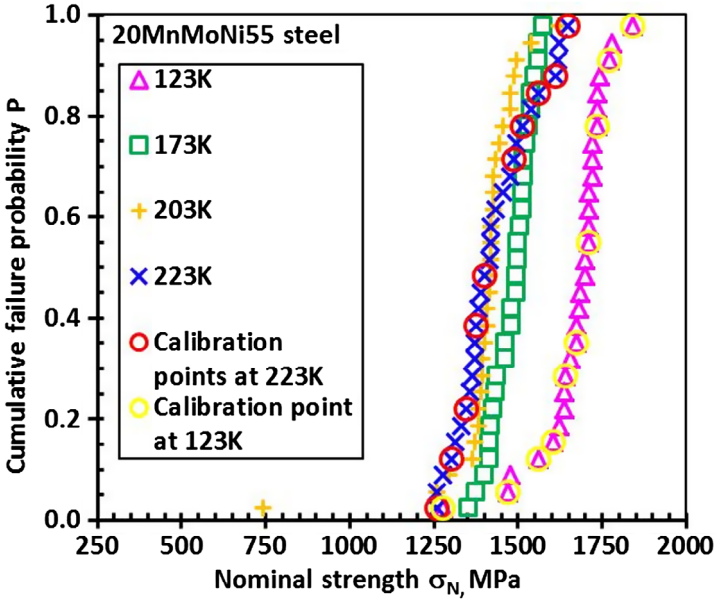

Figure 5. (Colour online) Weibull distribution plots of experimental fracture strength data σ_N of 20MnMoNi55 steel [53]. Note that the 10 circled points each at 123 and 223 K are used for FE simulations.

Table 5. Summary of Weibull calibration results by this study and in Refs. [52,53].

	This study		Ref. [52]		Ref. [53]	
	New model Equation (20)		Beremin model Equation (1)		Empirical Weibull model Equation (39)	
T (K)	m	σ_0 (MPa)	m	σ_0 (MPa)	m	σ_0 (MPa)
223	10.25	1663.5	37.2	2201	15.1	2014
203	/	/	/	/	22.1	1455
173	/	/	37.1	2460	31.5	1504
123	9.82	1879.2	15.7	3509	17.2	1670

5. FE analysis and calibration procedure

5.1. General description

In this work, FE simulations are conducted by ABAQUS 6.14for the 3D notched specimens tested in [52,53]. Due to symmetry considerations, only one-eighth of the specimen is modelled, as embedded in Figure 2 and also shown as Figure 6. The 20-node brick elements (quadratic elements, C3D20R) are used. The number of elements and nodes are about 145,807 and 607,860, respectively. The nominal fracture strength σ_N which is based on the net section area at the notch (in the symmetrical plane normal to the loading axis) is equivalently transformed into the remote loading stress σ_∞ via the relationship $\sigma_\infty = \sigma_N \left(\emptyset_2/\emptyset_1\right)^2$, with $\emptyset_1 = 14\,\text{mm}, \emptyset_2 = 7.7\,\text{mm}$ (Figure 2), as depicted by the red stress vectors also in Figure 6. The back-calculated remote loading stresses are in the range of

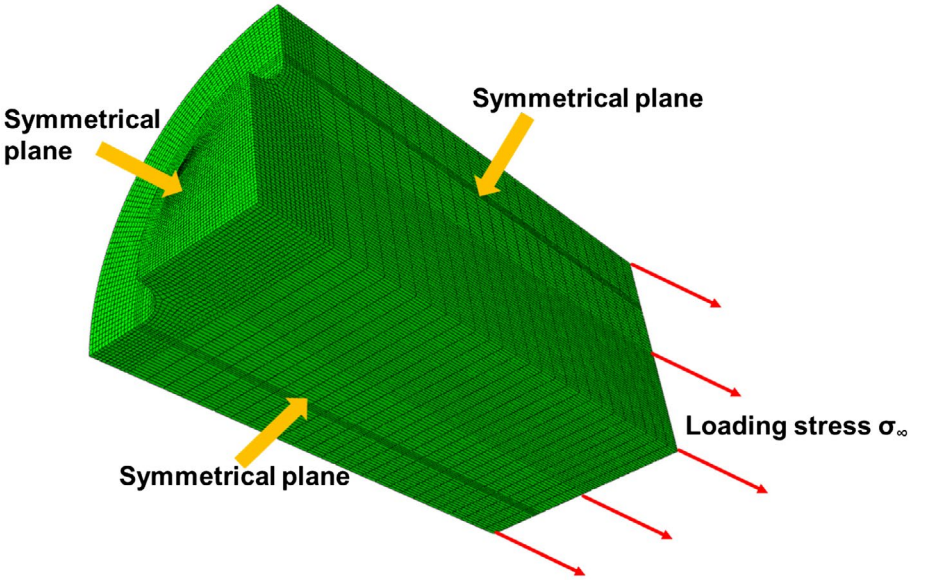

Figure 6. (Colour online) FE modelling for one-eighth of the notched specimens.

380.9–498.6 MPa for specimens tested at 223 K and 386.5–556.5 MPa at 123 K, respectively. FE modelling is performed at 223 and 123 K. Although 30 specimens were tested at each temperature, due to the large amount of computation effort involved at each load, instead of performing FE calculation at each loading point, we chose to uniformly pick only ten loads out of the 30 fracture loads for FE simulations at each temperature, as shown by the circled dots in Figure 5. The demanded material constitutive properties for FE simulations including the Young's modulus E, the Poisson's ratio ν, and the temperature-dependent plastic flow curves are collectively given in Table 4 and Figure 4.

5.2. Calibration procedure

This work will evaluate the new statistical model in Equation (20), with σ_W defined in Equation (21). Once σ_W is calculated according to Equation (21), Equation (22) is called in to estimate the two parameters (m and σ_0). Methods to calibrate Equation (22) are well developed [7–14], with either the maximum likelihood method or the linear regression method being used. Therefore, the novelty and the key point to estimate m and σ_0 for Equation (20) is to properly and efficiently evaluate the threshold stress $\sigma_{1,0}$ for the initial yielding of a finite volume element ΔV to enable the calculation of the newly defined Weibull stress σ_W in Equation (21). Due to the non-uniform stress distributions in a notched specimen, each volume element can start plastic yielding at a different moment. Moreover, according to the von Mises yield criterion in Equation (13), the amplitude of the stress $\sigma_{1,0}$ for the initial yielding in each volume element can be different. We propose to

determine the value of $\sigma_{1,0}$ for each volume element using FE analysis by assuming the steel as an elastic-perfectly plastic material, which is defined by the Young's modulus E, Poisson's ratio ν, and yield stress σ_{ys}. The resultant value of stress σ_1 in a plastically deformed volume element is taken as $\sigma_{1,0}$ for that particular volume element. A subroutine is written to extract the stress and strain distributions for different elements. It should be noted that due to the converging difficulty with an elastic-perfectly plastic material, the loading stresses of 280 MPa at 223 K and 380 MPa at 123 K are applied on the specimen to calculate $\sigma_{1,0}$ at the corresponding temperatures. These loading stresses are sufficient to induce yielding in nearly all the actual region in the specimen for volume integration to calculate the Weibull stress σ_W in Equation (21). Next, the routine FE analysis is conducted using the true stress–strain curve of the real material with plastic hardening behaviour in Figure 4, to calculate the stress σ_1 in each volume element at a given load. As the third step, the newly defined Weibull stress σ_W is calculated by substituting the values of the instant stress σ_1 at a given load and the threshold stress $\sigma_{1,0}$ for exactly the same volume element one by one into Equation (21). In consistence with the common practice for the similar materials, the reference volume V_0 is taken as 0.001 mm^3 in this calculation. This process is repeated at each load to obtain the corresponding values of σ_W as input to Equation (22). Then the same conventional calibration procedure as used in [7–14] is applied to obtain the values of m and σ_0. The flow chart for the described calibration procedure is presented in Figure 7. This proposed calibration procedure is validated in [54, 55].

6. Results and analysis

6.1. Stress distributions in the specimen

Figure 8 shows the von-Mises stress (σ_{VM}) distributions in the specimen subjected to different loadings tested at 123 K, for both the realistic plastic hardening behaviour and the elastic-perfectly-plastic behaviour of the steel. Corresponding results of FE analysis at 223 K are provided in Figure 9. The von-Mises stress distributions are used to determine the plastic volume V_{pl} involved in Weibull stress calculation according to Equation (21). By definition, the volume V_{pl} encompasses all plastic deformation region with $\sigma_1 \geq \sigma_{1,0}$. For this specific round notched tensile bar specimen, $\sigma_{1,0} \geq \sigma_{ys}$. The extreme condition of $\sigma_{1,0} = \sigma_{ys}$ can be achieved in the wider section far away from the notch section, e.g. Point A in Figure 2. However, to reduce FE computation time for the realistic material constitutive behaviour, in this study, the integral volume V_{pl} is defined as the volume with Von-Mises stress (σ_{VM}) higher than 1.5 $\sigma_{ys,}$ i.e. $\sigma_{VM} \geq 1.5\sigma_{ys}$, with the expectation to only induce a very minor error. Figure 10 presents the distributions of $\sigma_{1,0}$ on the modelled specimen at 223 K (a) and 123 K (b), respectively.

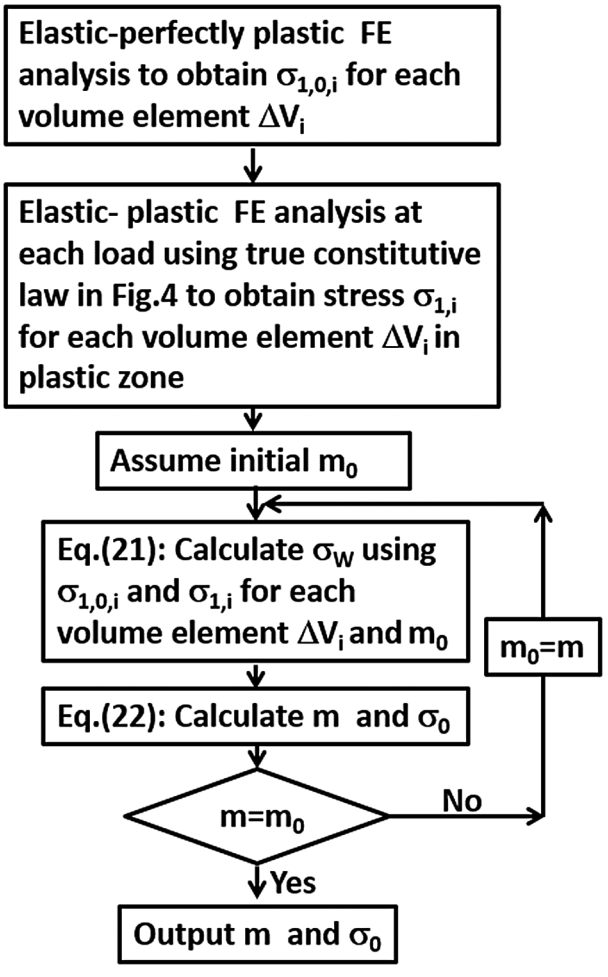

Figure 7. Flowchart for the calibration procedure of the new statistical model in Equation (20) at each temperature.

6.2. Results of calibration

The calibrated values of two model parameters (m and σ_0) at 223 and 123 K are summarised in Table 5. As expected, both parameters show very weak temperature dependence for a change of temperature by 100 K. Specifically, m = 10.25 at 223 K and m = 9.82 at 123 K, with an average value m = 10.03; σ_0 = 1663.5 MPa at 223 K and σ_0 = 1879.2 MPa at 123 K, with an average value σ_0 = 1771.3 MPa. In other words, within the temperature range from 223 K to 123 K, for every 10 K change in temperature, there is only 0.2% change in the value of m and 0.6% change in σ_0. Even the overall difference in the absolute values of σ_0 from 223 to 123 K is only 108 MPa, which is quite small. Nevertheless, we believe it is beneficial to understand the possible root causes for this minor variation in σ_0 for future studies. First, at each temperature, we only adopted 10 out of 30 external loads for model calibration. Obviously, more stable calibration results are expected when

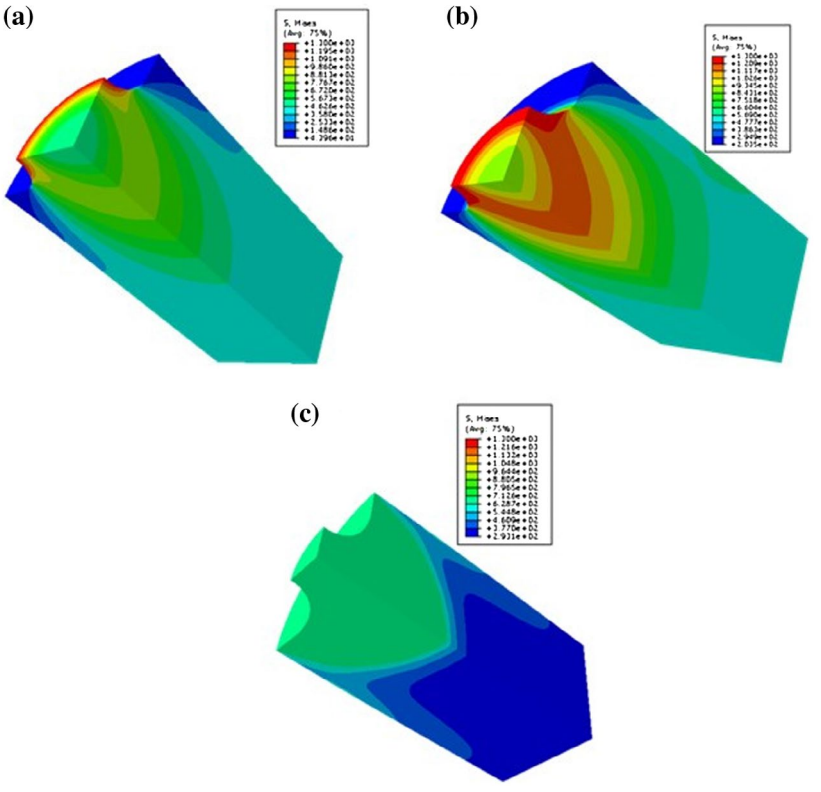

Figure 8. (Colour online) Examples of von-Mises stress distributions for the notched specimens at 123 K. (a) $\sigma_\infty = 386$ MPa (Corresponding to $\sigma_N = 1277$ MPa), true elastic-plastic hardening constitutive law for the steel; (b) $\sigma_\infty = 556$ MPa (corresponding to $\sigma_N = 1839$ MPa), true elastic-plastic hardening constitutive law for the steel; (c) $\sigma_\infty = 380$ MPa (corresponding to $\sigma_N = 1256$ MPa), elastic-perfectly plastic constitutive model.

using more data points. Second, the approximate evaluation of plastic volume V_{pl} is also responsible. As mentioned in Section 5, in order to reduce some computation time in the FE analysis, we adopted the criterion $\sigma_{VM} \geq 1.5\sigma_{ys}$ instead of the more accurate one $\sigma_{VM} \geq \sigma_{ys}$to calculate the volume of plastic zone V_{pl}, as input for calculating the Weibull stress σ_W using Equation (21). This will only result in a slight underestimate of the plastic volume V_{pl}, and in turn, lead to a smaller value of the Weibull stress σ_W than its true value. As an example, Figure 11 compares the volume of plastic zone V_{pl} calculated by the two approaches at 123 K, in which $V_{pl}(\sigma_{VM} \geq \sigma_{ys})$ refers to the volume of plastic zone determined by strictly adhering to the von Mises yielding criterion $\sigma_{VM} \geq \sigma_{ys}$, while $V_{pl}(\sigma_{VM} \geq 1.5\sigma_{ys})$, which is adopted in this study, denotes the volume of plastic zone determined according to $\sigma_{VM} \geq 1.5\sigma_{ys}$. The difference in the values of the two volumes seems to be pretty significant. However, the reader is reminded that in the calculation of Weibull stress σ_W using Equation (21), it is the product term for each volume element ΔV_i, $(\sigma_1 - \sigma_{1,0})^m \Delta V_i$, instead of the volume element ΔV_i itself, plays the key role. If the amount of the product terms $(\sigma_1 - \sigma_{1,0})^m \Delta V_i$ within the ignored portion of the

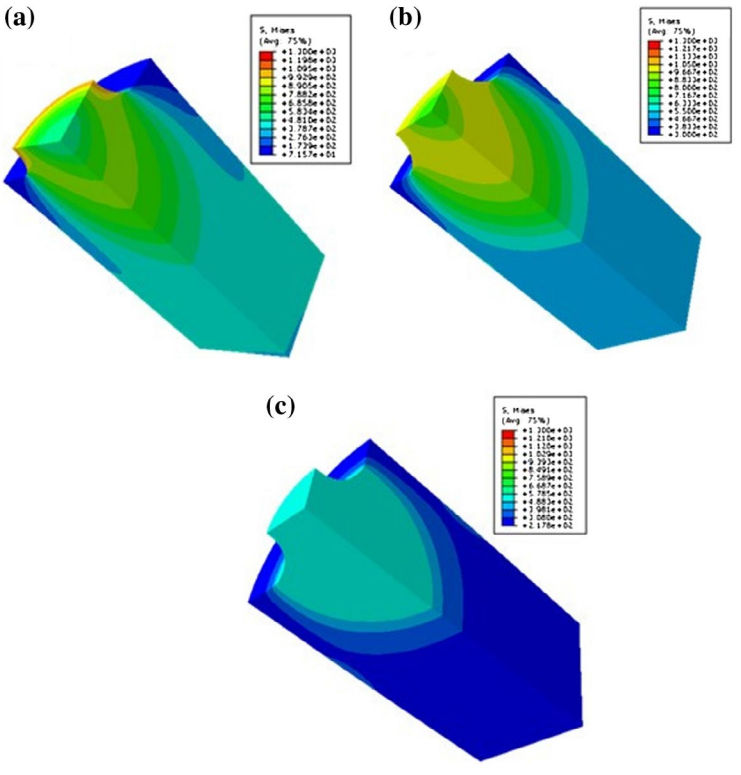

Figure 9. (Colour online) Examples of von-Mises stress distributions in the notched specimens at 223 K: (a) $\sigma_\infty = 380$ MPa (corresponding to $\sigma_N = 1259$ MPa), true elastic-plastic hardening constitutive law for the steel; (b) $\sigma_\infty = 498$ MPa (corresponding to $\sigma_N = 1648$ MPa), true elastic-plastic hardening constitutive law for the steel; (c) $\sigma_\infty = 280$ MPa (corresponding to $\sigma_N = 926$ MPa), elastic-perfectly plastic constitutive model.

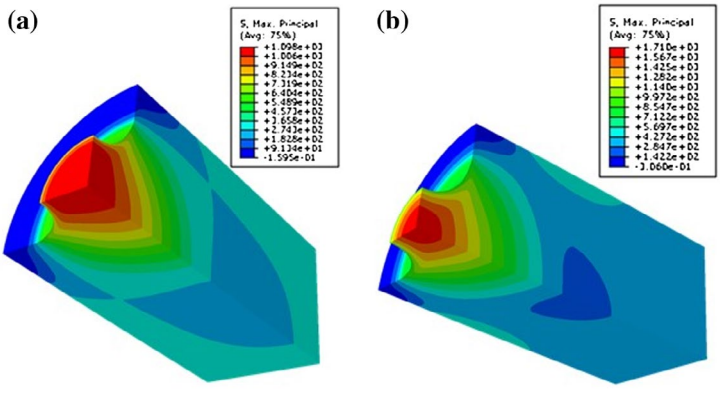

Figure 10. (Colour online) The distributions of $\sigma_{1,0}$ in the specimen at 223 K (a) and 123 K (b), respectively, based on the elastic-perfectly plastic constitutive model.

plastic volume, here denoted as $V_{pl}(\sigma_{ys} \le \sigma_{VM} \le 1.5\sigma_{ys})$, is insignificant compared to the total summation $\sum(\sigma_1 - \sigma_{1,0})^m \Delta V_i$, the final impact on the calibration result should not be a concern. To better elaborate this point, we compared the

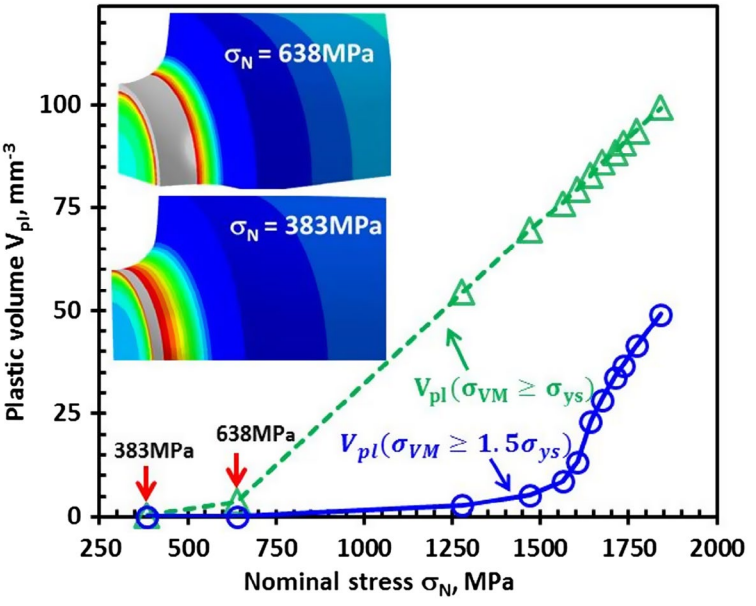

Figure 11. (Colour online) Variation of the volume of plastic zone Vpl with nominal stress σ_N at 123 K. Note that $V_{pl}(\sigma_{VM} \geq \sigma_{ys})$ refers to the volume of plastic zone determined by strictly adhering to the von Mises yielding criterion $\sigma_{VM} \geq \sigma_{ys}$, while $V_{pl}(\sigma_{VM} \geq 1.5\sigma_{ys})$, which is adopted in this study, denotes the volume of plastic zone determined according to $\sigma_{VM} \geq 1.5\sigma_{ys}$. The tiny grey area in the embedded charts for von-Mises stress distributions is the plastic deformation zone.

plastic volume, the corresponding Weibull stress, and subsequently the cumulative failure probability P at two much lower nominal strength values ($\sigma_N = 383$ MPa, 638 MPa), which correspond to 30 and 50% of the minimum value (1382 MPa) of the 30 reported nominal fracture strength data at 123 K (see Figure 5). The stress distributions at both strength values are embedded in Figure 11, with the grey areas being the plastic deformation zone. See Figure 12 for more detailed results. The results are summarised in Table 6. On one hand, at both nominal strengths ($\sigma_N = 383$ MPa, 638 MPa), the criterion $\sigma_{VM} \geq 1.5\sigma_{ys}$ resulted in zero valued plastic volume and hence the Weibull stress, translating into zero cumulative failure probability ($P = 0$). On the other hand, at the nominal strength $\sigma_N = 383$ MPa, the strict execution of von Mises yielding criterion ($\sigma_{VM} \geq \sigma_{ys}$) leads to Weibull stress $\sigma_W = 20.1$ MPa, or $(\sigma_W/\sigma_0)^m = 1.42 \times 10^{-27}$, which gives the cumulative failure probability $P = 0$, while $\sigma_N = 638$ MPa results in the cumulative failure probability $P = 5.38 \times 10^{-6}$.

6.3. Analysis: validation of temperature independence of two model parameters

6.3.1. 20MnMoNi55 steel

In principle, with the two model parameters being calibrated above, the new model in Equation (20) is now fully transparent and can be used for simulating and predicting cleavage fracture induced failures in real applications in aid of FE

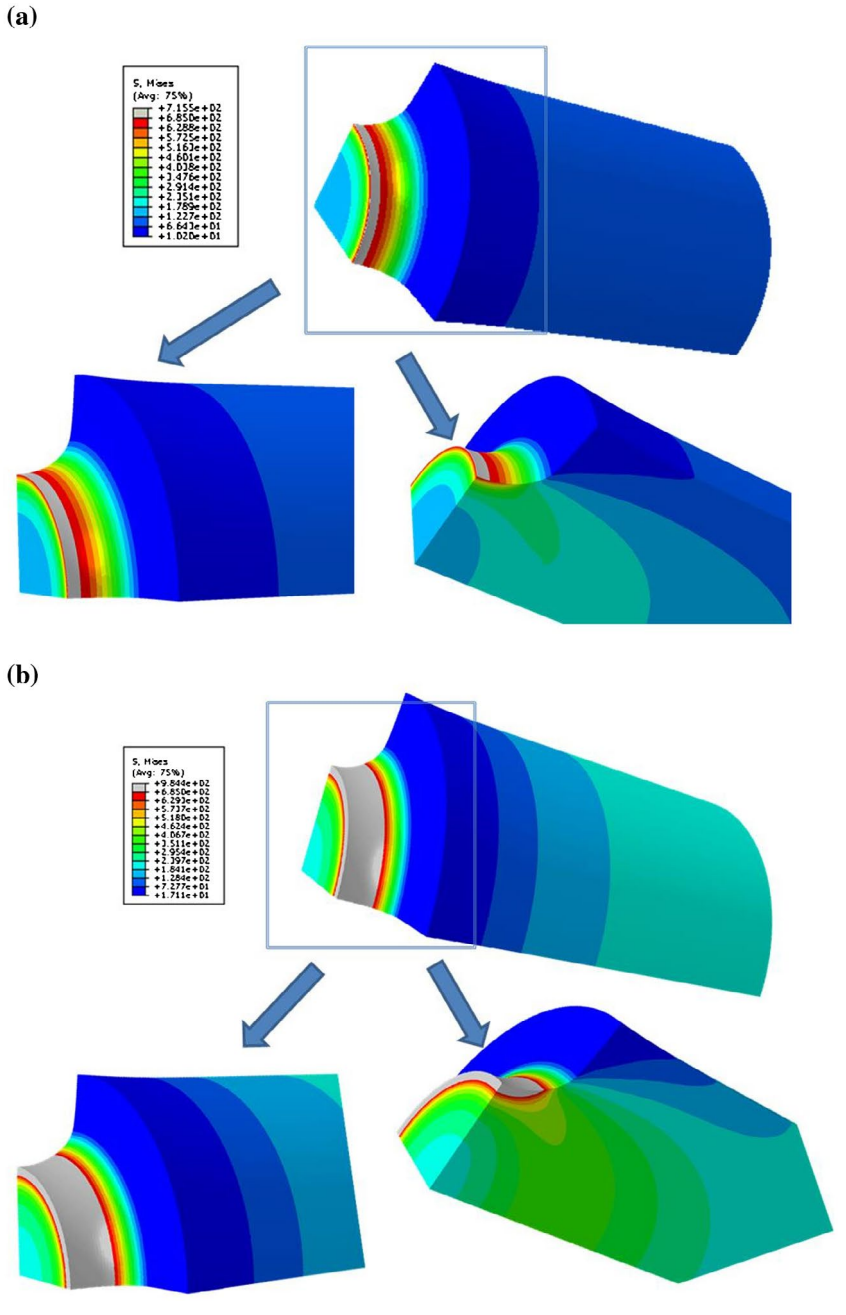

Figure 12. (Colour online) von-Mises stress distributions for the notched specimens at 123 K. (a) $\sigma_N = 383$ MPa and (b) $\sigma_N = 638$ MPa, true elastic-plastic hardening constitutive law for the steel. The tiny grey area is the plastic deformation zone.

analysis. However, since the major interest of this work is to justify the temperature independence of the two parameters m and σ_0 in the new model (Equation (20)), here below we will pursue a different path based on current FE results instead of resorting to further FE analysis to analyse the experimental data in Figure 5.

Table 6. Results of plastic volume (V_{pl}) and Weibull stress σ_W determined by $\sigma_{VM} \geq \sigma_{ys}$ and $\sigma_{VM} \geq 1.5\sigma_{ys}$.

	Nominal fracture strength $\sigma_N = 383$ MPa			Nominal fracture strength $\sigma_N = 638$ MPa		
Criterion	V_{pl}, mm^{-3}	σ_W, MPa	P, Equation (20)	V_{pl}, mm^{-3}	σ_W, MPa	P, Equation (20)
$\sigma_{VM} \geq \sigma_{ys}$	0.24	20.1	0	3.66	526.4	5.38×10^{-6}
$\sigma_{VM} \geq 1.5\sigma_{ys}$	0	0	0	0	0	0

Assume $m = 10$, $\sigma_0 = 1771$ MPa for calculating cumulative failure probability P

By definition in Equation (21), the new Weibull stress σ_W is affected by material constitutive properties including elastic properties (E, ν), yield stress σ_{ys} and plastic hardening parameters, specimen geometry which dictates constraint effect, Weibull modulus m, and external load represented by the nominal stress at notch section σ_N. For a given specimen geometry such as the round notched tensile bar in this study, at a fixed temperature (T), the new Weibull stress σ_W should only vary with m and σ_N, that is,

$$\sigma_W(T) = f(m, \sigma_N) \tag{40}$$

Within the relatively narrow temperature range susceptible for cleavage fracture, out of all the material constitutive properties, only the yield stress σ_{ys} has pronounced temperature dependence. Now if we assume that the Weibull modulus m is also temperature independent, Equation (40) can be converted to a normalised format that allows considering temperature effect:

$$\frac{\sigma_W}{\sigma_{ys}} = \frac{\sigma_W(T)}{\sigma_{ys}(T)} = f\left(\frac{\sigma_N(T)}{\sigma_{ys}(T)}\right) \tag{41}$$

Equation (41) suggests that there exists a 'master curve' that correlates the two normalised variables $\frac{\sigma_W}{\sigma_{ys}}$ and $\frac{\sigma_N}{\sigma_{ys}}$ at different temperatures. However, further work is demanded to understand the exact expression of function $y = f(x)$. For conservation, we expect $f(x)$ is a non-linear function, but it is possible to be approximated by a linear one within certain loading regime.

Specific to current study, Figure 13 summarises the correlation between the nominal fracture strength σ_N and the corresponding new Weibull stress σ_W (Equation (21)) at 223 and 123 K. Both σ_N and σ_W are normalised by the yielding stress σ_{ys} at the corresponding temperature. As shown in Figure 13, these 20 data points show a strong linear correlation between the normalised new Weibull stress σ_W/σ_{ys} and the normalised nominal strength σ_N/σ_{ys}. However, we take this result as a strong justification on the 'master curve' behaviour more than on emphasising the linearity of correlation.

Now, substitution of Equation (41) in the new model Equation (20) leads to

$$P = 1 - \exp\left[-\left(\frac{\sigma_{ys}}{\sigma_0}\right)^m f^m\left(\frac{\sigma_N}{\sigma_{ys}}\right)\right] \tag{42}$$

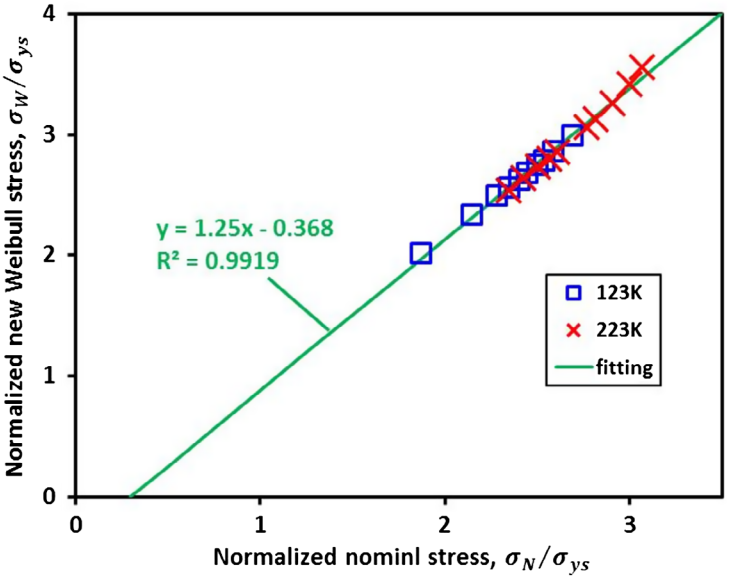

Figure 13. (Colour online) Correlation between the normalised nominal strength σ_N/σ_{ys} and the normalised new Weibull stress σ_W/σ_{ys}.

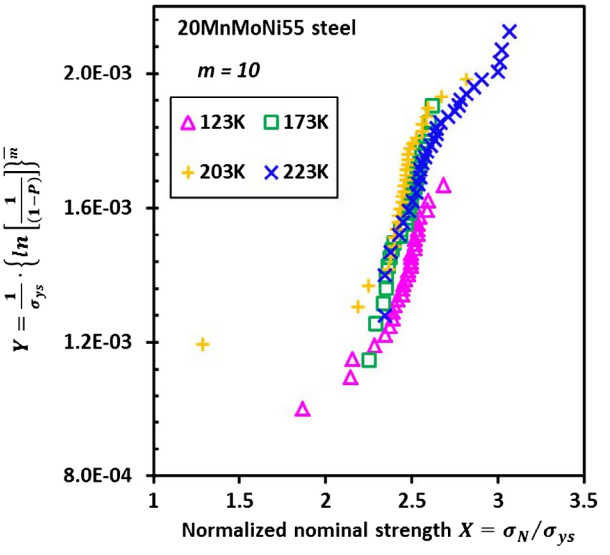

Figure 14. (Colour online) Correlation between the compound parameters $Y = \frac{1}{\sigma_{ys}} \cdot \left\{ ln\left[\frac{1}{(1-P)}\right]\right\}^{\frac{1}{m}}$ and $X = \frac{\sigma_N}{\sigma_{ys}}$ at four different temperatures.

or in equivalence,

$$Y = \frac{1}{\sigma_{ys}} \cdot \left\{ ln\left[\frac{1}{(1-P)}\right]\right\}^{\frac{1}{m}} = \frac{1}{\sigma_0} \cdot f\left(\frac{\sigma_N}{\sigma_{ys}}\right) \tag{43}$$

If the function $y = f(x)$ is a linear function as shown in Figure 13, according to Equation (43), there will be a linear correlation between $Y = \frac{1}{\sigma_{ys}} \cdot \left\{ ln\left[\frac{1}{(1-P)}\right] \right\}^{\frac{1}{m}}$ and $X = \frac{\sigma_N}{\sigma_{ys}}$.

Equation (43) permits us to transfer the experimental data in Figure 5 into Figure 14 for the expected correlation between the compound parameters $Y = \frac{1}{\sigma_{ys}} \cdot \left\{ ln\left[\frac{1}{(1-P)}\right] \right\}^{\frac{1}{m}}$ and $X = \frac{\sigma_N}{\sigma_{ys}}$ with the calibrated value $m = 10$ and

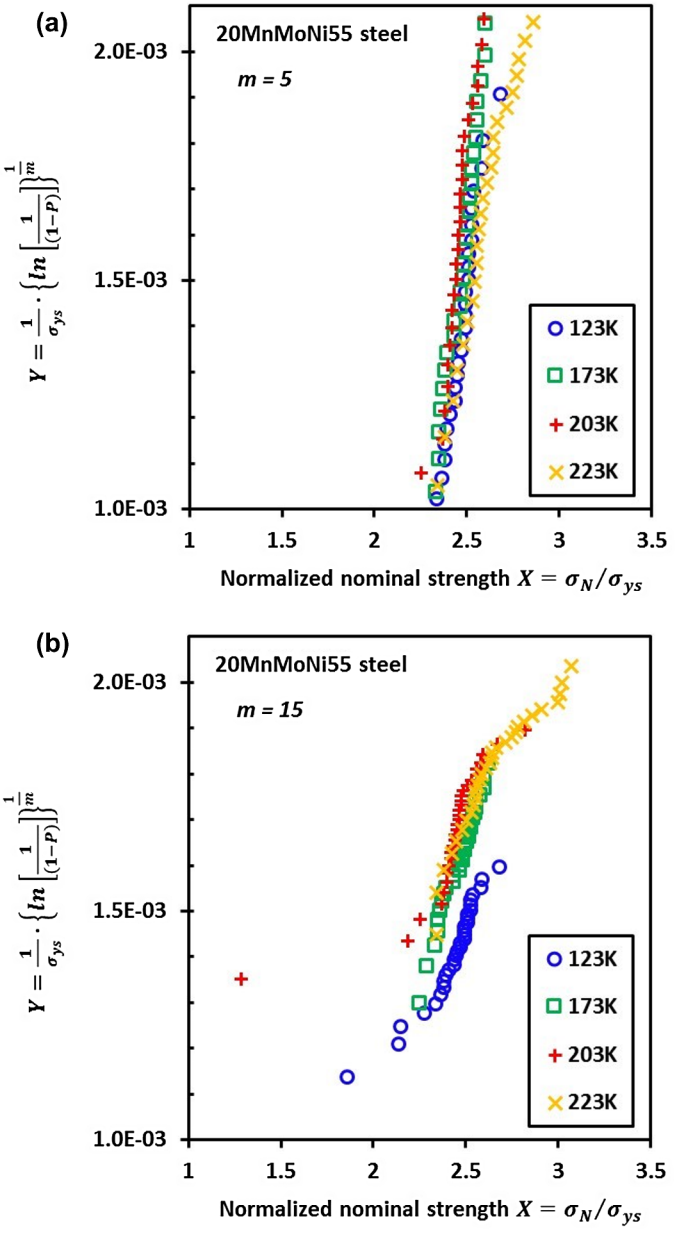

Figure 15. (Colour online) Correlation between the compound parameters $Y = \frac{1}{\sigma_{ys}} \cdot \left\{ ln\left[\frac{1}{(1-P)}\right] \right\}^{\frac{1}{m}}$ and $X = \frac{\sigma_N}{\sigma_{ys}}$ at four different temperatures: (a) $m = 5$; (b) $m = 15$.

temperature dependence of yield stress in Table 5. Three observations can be made on Figure 14: First, the 'master curve' behaviour of the 120 data points is revealed, providing convincing validation to the temperature independence of Weibull parameters m and σ_0. Second, with 120 data points as input, the correlation between the two compound parameters Y and X takes a S-shaped transition curve instead of a straight line. This reminds us to be very careful about the linear fitting

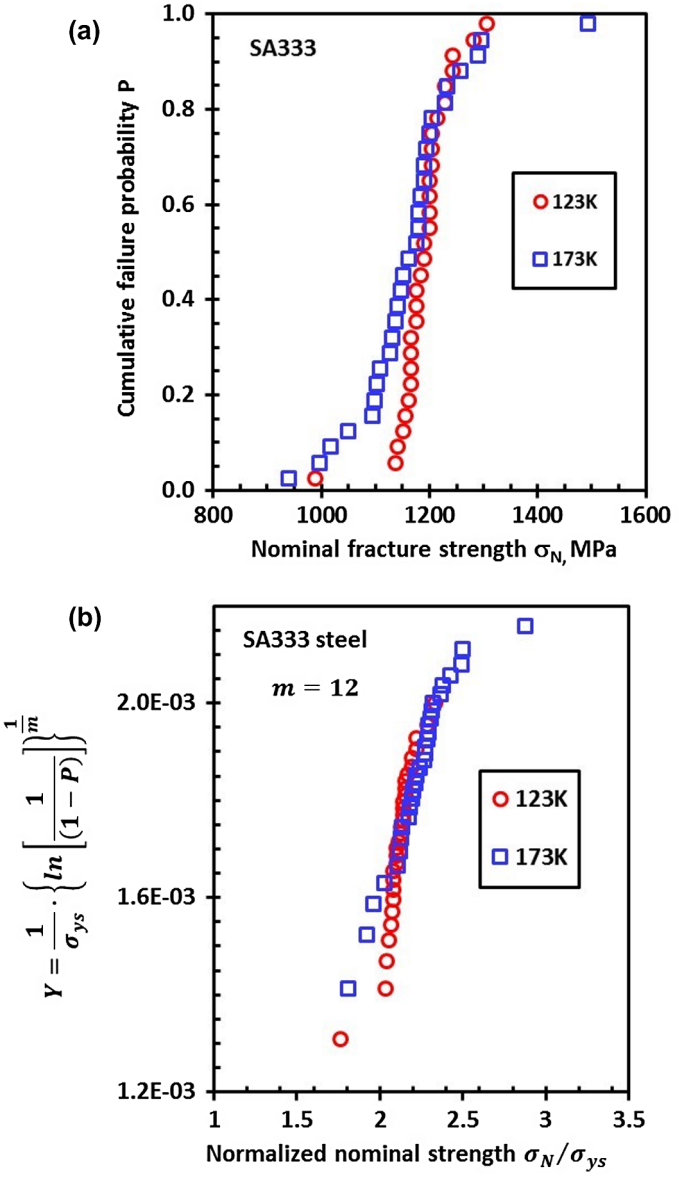

Figure 16. (Colour online) Analysis of strength data of SA 333 steel: (a) Weibull distribution plots of experimental fracture strength data σ_N [53]; (b) Correlation between the compound parameters $Y = \frac{1}{\sigma_{ys}} \cdot \left\{ ln\left[\frac{1}{(1-P)}\right] \right\}^{\frac{1}{m}}$ and $X = \frac{\sigma_N}{\sigma_{ys}}$.

of much less data in Figure 14. Third, the tight distribution of experimental data also tells that the calibrated value $m = 10$ is pretty accurate. To further highlight this point, the scenarios of $m = 5$ and $m = 15$ are plotted in Figure 15(a) and (b) for comparison.

To further elaborate the temperature independence of Weibull parameters m and σ_0 underpinning the 'master curve' behaviour between the compound parameters $Y = \frac{1}{\sigma_{ys}} \cdot \left\{ ln\left[\frac{1}{(1-P)}\right] \right\}^{\frac{1}{m}}$ and $X = \frac{\sigma_N}{\sigma_{ys}}$ at four different temperatures, let's examine two additional examples.

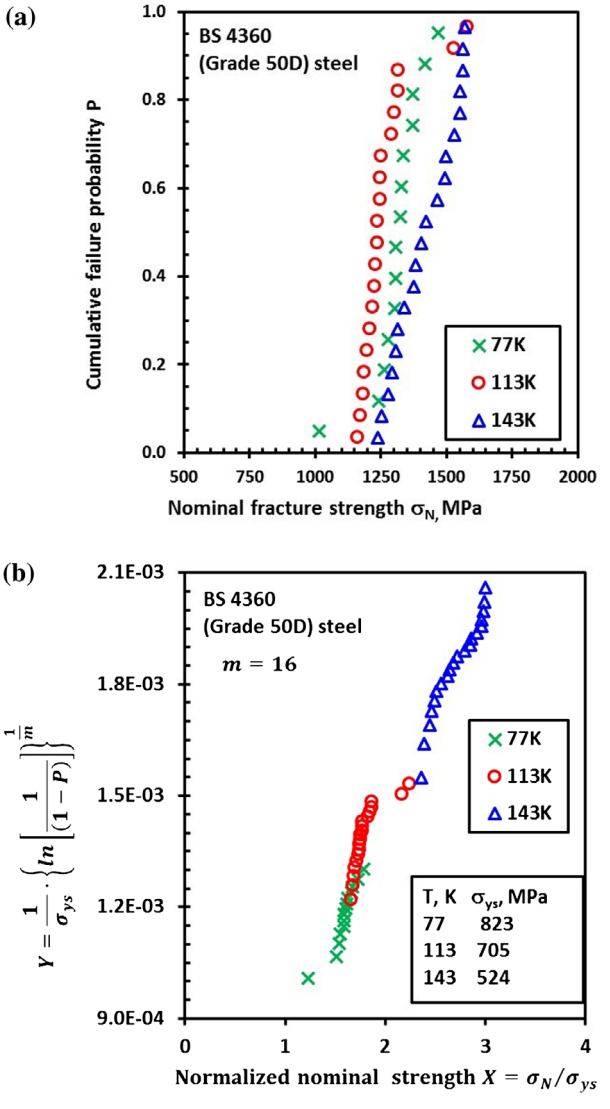

Figure 17. (Colour online) Analysis of strength data of BS 4360 (Grade 50D) steel: (a) Weibull distribution plots of experimental fracture strength data σ_N [8]; (b) Correlation between the compound parameters $Y = \frac{1}{\sigma_{ys}} \cdot \left\{ ln\left[\frac{1}{(1-P)}\right] \right\}^{\frac{1}{m}}$ and $X = \frac{\sigma_N}{\sigma_{ys}}$.

6.3.2. SA333 (Grade 6) steel

In [53], the nominal fracture strength σ_N data for SA333 steel were also measured at 123 K and 173 K as presented in the form of the Weibull distribution plot in Figure 16(a).The yield stress values at these two temperatures are given in Table 1. Similar to the case of 20MnMoNi55 steel, we can also transform the data in Figure 16(a) into the correlation between the two compound parameters in Figure 16(b). Since we have not performed FE analysis to calibrate Weibull parameters m and σ_0 for this steel, the value of m adopted in Figure 16(b) is obtained by trials and errors. Although eventually we'll need to take stricter FE analysis to calibrate the two model parameters, the approach we take here is sufficient to be used for justifying the existence of the 'master curve' behaviour in this steel.

6.3.3. BS 4360 (Grade 50D) steel

Figure 17(a) shows the nominal fracture strengthσ_N data of BS 4360 (Grade 50D) steel measured on circumferentially notched round tensile specimens by Wiesner an Goldthorpe [8]. In the absence of FE analysis to calibrate Weibull parameters m and σ_0 for this steel, m = 16 is adopted to transform the data in Figure 17(a) into the correlation between the compound parameters in Figure 17(b). Evidently, there seems also to be a 'master curve' synchronising all the experimental data in this steel.

7. Summary and conclusions

Since early 1980s when the Beremin model was proposed, the dependence of temperature and specimen geometry on the parameters m and σ_0 for the Beremin model and other LA models for cleavage fracture has been a continuous subject of debate. In this work, a new LA model to cleavage fracture, which is formulated strictly to abide by both probability theory and physical understanding of cleavage mechanisms, is adopted to investigate the effect of temperature on the parameters m and σ_0. The consistency of the new LA model to the generic LA methodology and its differences with some typical existing models are interpreted. Specifically, the work relies on a set of published experimental data obtained from notched tension specimens, a recently developed calibration procedure for this new LA model by the authors [54, 55], and a series of FE calculations of stress distributions. Based on this study, the following conclusions are drawn:

(1) A method to calculate the maximum principal tensile stress $\sigma_{1,0}$ on a volume element at the occurrence of its initial plastic yielding is validated based on FE method. The value of $\sigma_{1,0}$ varies with volume element and temperature.
(2) Calibration results show that the two parameters m and σ_0 in the new LA model are temperature independent from 123 to 223 K.

(3) The one-to-one correlation between the normalised new Weibull stress and the normalised nominal strength leads to the finding of a master curve characteristic that synchronises the variation of cleavage fracture probability with external loading at different temperatures. This provides a new avenue to calculate cleavage fracture probability with reduced FE efforts.

Our next effort is to adopt this new LA model to investigate the effect of specimen geometry on the two model parameters which includes fracture toughness specimens. Due to the dependence of critical event for cleavage fracture on stress state, certain changes of critical event from a notched specimen to a cracked specimen are expected. The corresponding impact on model parameters will be explored.

Acknowledgements

The new local approach was initiated due to a research stay with Humboldt Research Fellowship in Institute of Ferrous Metallurgy (IEHK) at RWTH Aachen University. Wei-Sheng Lei is grateful to Professor Winfried Dahl and Professor Wolfgang Bleck for hosting the visit and the Alexander von Humboldt Foundation for the financial support. The support by the State Key Laboratory for Strength and Vibration of Mechanical Structures, Xi'an Jiaotong University is greatly acknowledged.

Disclosure statement

No potential conflict of interest was reported by the authors.

Funding

Guian Qian and Markus Niffenegger are grateful for the financial support of the PROBAB Project by the Swiss Federal Nuclear Safety Inspectorate (ENSI) (DIS-Vertrag Nr. H-100668).

References

[1] W.-S. Lei, *A framework for statistical modeling of plastic yielding initiated cleavage fracture of structural steels*, Philos. Mag. 96 (2016), pp. 3586–3631.
[2] W.-S. Lei, *A cumulative failure probability model for cleavage fracture in ferritic steels*, Mech. Mater. 93 (2016), pp. 184–198.
[3] W.-S. Lei, On the statistical modeling of cleavage fracture toughness of structural steels, Mech. Mater. 101 (2016), pp. 81–92.
[4] G. Qian and M. Niffenegger, *Deterministic and probabilistic analysis of a reactor pressure vessel subjected to pressurized thermal shocks*, Nucl. Eng. Des. 273 (2014), pp. 381–395.
[5] G. Qian, V.F. González-Albuixech, and M. Niffenegger, *Probabilistic PTS analysis of a reactor pressure vessel by considering realistic crack distributions*, Nucl. Eng. Des. 270 (2014), pp. 312–324.
[6] J.D. Landes and D.H. Shaffer, *Statistical characterization of fracture in the transition region*, in *Proceedings of the Twefth Conferene on Fracture Mechanics, ASTM STP 700*, J.G. Kaufman, ed., American Society for Testing and Materials, Baltimore, 1980, pp. 368–382.

[7] F.M. Beremin, *A local approach for cleavage fracture of a nuclear pressure vessel steel*, Metall. Trans. A 14 (1983), pp. 2277–2287.
[8] C.S. Wiesner and M.R. Goldthorpe, *The effect of temperature and specimen geometry on the parameters of the 'Local Approach' to cleavage fracture*, J. de Phys. IV 6 (1996), pp. 295–304.
[9] K. Hojo, I. Muroya, and A. Brückner-Foit, *Fracture toughness transition curve estimation from a notched round bar specimen using the local approach method*, Nucl. Eng. Des. 174 (1997), pp. 247–258.
[10] S. Hadidi-Moud, A. Mirzaee-Sisan, C.E. Truman, and D.J. Smith, *A local approach to cleavage fracture in ferritic steels following warm pre-stressing*, Fatigue Fract. Eng. Mater. Struct. 27 (2004), pp. 931–942.
[11] X. Gao, G. Zhang, and T.S. Srivatsan, Prediction of cleavage fracture in ferritic steels: A modified Weibull stress model, Mater. Sci. Eng. A 394 (2005), pp. 210–219.
[12] J.P. Petti and R.H. Dodds, *Calibration of the Weibull stress scale parameter, σu, using the Master Curve*, Eng. Fract. Mech. 72 (2005), pp. 91–120.
[13] A. Pineau, *Development of the local approach to fracture over the past 25 years: Theory and applications*, Int. J. Fract. 138 (2006), pp. 139–166.
[14] G.A. Qian, V.F. González-Albuixech, and M. Niffenegger, *Calibration of Beremin model with the master curve*, Eng. Fract. Mech. 136 (2015), pp. 15–25.
[15] C. Ruggieri and R.H. Dodds, *An engineering methodology for constraint corrections of elastic-plastic fracture toughness – Part I: A review on probabilistic models and exploration of plastic strain effects*, Eng. Fract. Mech. 134 (2015), pp. 368–390.
[16] M. Moattari, I. Sattari-Far, I. Persechino, and N. Bonora, *Prediction of fracture toughness in ductile-to-brittle transition region using combined CDM and Beremin models*, Mater. Sci. Eng. A 657 (2016), pp. 161–172.
[17] W.-S. Lei, *A statistical model of cleavage fracture in structural steels with power-law distribution of microcrack size*, Philos. Mag. Lett. 96 (2016), pp. 101–111.
[18] J. Heerens, M. Pfuff, D. Hellmann, and U. Zerbst, *The lower bound toughness procedure applied to the Euro fracture toughness dataset*, Eng. Fract. Mech. 69 (2002), pp. 483–495.
[19] W.-S. Lei, *A discussion of 'An engineering methodology for constraint corrections of elastic–plastic fracture toughness – Part II: Effects of specimen geometry and plastic strain on cleavage fracture predictions' by C. Ruggieri, R.G. Savioli, R.H. Dodds [Eng. Fract. Mech. 146 (2015) 185–209]*, Eng. Fract. Mech. 178(2017) (2015), pp. 527–534.
[20] W.-S. Lei, *Evaluation of the basic formulations for the cumulative probability of brittle fracture with two different spatial distributions of microcracks*, Fatigue Fract. Eng. Mater. Struct. 39 (2016), pp. 611–623.
[21] T. Lin, A.G. Evans, and R.O. Ritchie, *A statistical model of brittle fracture by transgranular cleavage*, J. Mech. Phys. Solids 34 (1986), pp. 477–497.
[22] D.M. Li and M. Yao, *A metallographic and fractographic study of the origin of cleavage fracture in mild steel*, Mater. Charact. 36 (1996), pp. 27–33.
[23] D.M. Li and M. Yao, *Modeling a cleavage-characteristic stress (Sc0) of ferritic steels*, in *George R. Irwin Symposium on Cleavage Fracture*, Kwai S. Chan, ed., The Minerals, Metals & Materials Society, Warrendale, PA, 1997, pp. 193–205.
[24] J.H. Chen, G.Z. Wang, and Q. Wang, *Change of critical events of cleavage fracture with variation of microscopic features of low-alloy steels*, Metall. Mater. Trans. A 33 (2002), pp. 3393–3402.
[25] S.R. Bordet, A.D. Karstensen, D.M. Knowles, and C.S. Wiesner, *A new statistical local criterion for cleavage fracture in steel. Part I: Model presentation*, Eng. Fract. Mech. 72 (2005), pp. 435–452.
[26] S. Kotrechko, *The key problems of local approach to cleavage fracture*, J. Theor. Appl. Mech. 51 (2013), pp. 75–89.

[27] M. Scibetta, *A cleavage fracture framework: New perspectives in cleavage modeling of ferritin steels*, Eng. Fract. Mech. 160 (2016), pp. 147–169.
[28] A. Pineau, A.A. Benzerga, and T. Pardoen, *Failure of metals I: Brittle and ductile fracture*, Acta Mater. 107 (2016), pp. 424–483.
[29] M. Mäntylä, A. Rossoll, I. Nedbal, C. Prioul, and B. Marini, *Fractographic observations of cleavage fracture intiation in a bainitic A508 steel*, J. Nucl. Mater. 264 (1999), pp. 257–262.
[30] T. Narström and M. Isacsson, *Microscopic investigation of cleavage initiation in modified A508B pressure vessel steel*, Mater. Sci. Eng. A 271 (1999), pp. 224–231.
[31] M.J. Balart, C.L. Davis, and M. Strangwood, *Cleavage initiation in Ti-V-N and V-N microalloyed ferritin-pearlitic forging steels*, Mater. Sci. Eng. A 284 (2000), pp. 1–13.
[32] A. Echeverría-Zubiría, M.A. Linaza, and J.M. Rodriguez-Ibabe, *Influence of microstructure on cleavage fracture initiation micromechanisms in steels*, in *13th European Conference on Fracture (ECF13): Fracture Mechanics: Applications and Challenges*, San Sebastián, September 6–9, 2000. Available at http://www.gruppofrattura.it/ocs/index.php/esis/ECF13/paper/viewFile/8530/4971
[33] J. Bošanský and T. Šmida, *Deformation twins-probable inherent nuclei of cleavage fracture in ferritic steels*, Mater. Sci. Eng. A 323 (2002), pp. 198–205.
[34] M.J. Balart, C.L. Davis, and M. Strangwood, *Observations of cleavage initiation at (Ti, V)(C, N) particles of heterogeneous composition in microalloyed steels*, Scripta Mater. 50 (2004), pp. 371–375.
[35] A. Echeverria and J.M. Rodriguez-Ibabe, *Cleavage micromechanisms on microalloyed steels. Evolution with temperature of some critical parameters*, Scripta Mater. 50 (2004), pp. 307–312.
[36] W.W. Bose Filho, A.L.M. Carvalho, and P. Bowen, *Micromechanisms of cleavage fracture initiation from inclusions in ferritin welds. Part II. Quantification of local fracture behavior observed in fatigue pre-cracked testpieces*, Mater. Sci. Eng. A 452–453 (2007), pp. 401–410.
[37] W.W. Bose Filho, A.L.M. Carvalho, and P. Bowen, *Micromechanisms of cleavage fracture initiation from inclusions in ferritin welds. Part I. Quantification of local fracture behavior observed in notched testpieces*, Mater. Sci. Eng. A 460–461 (2007), pp. 436–452.
[38] L. Lan, C. Qiu, H. Song, and D. Zhao, *Correlation of martensite-austenite constituent and cleavage crack initiation in welding heat affected zone of low carbon bainitic steel*, Mater. Lett. 125 (2014), pp. 86–88.
[39] S. Asako, T. Kawabata, S. Aihara, S. Kimura, and K. Kagehira, *Micro-processes of brittle fracture initiation in bainite steel manufactured by ausforming*, Procedia Structural Integrity 2 (2016), pp. 3668–3675.
[40] G.Z. Wang, Y.G. Liu, and J.H. Chen, *Investigation of cleavage fracture initiation in notched specimens of a C–Mn steel with carbides and inclusions*, Mater. Sci. Eng. A 369 (2004), pp. 181–191.
[41] J. He, J. Lian, G. Golisch, A. He, Y. Di, and S. Münstermann, *Investigation on micromechanism and stress state effects on cleavage fracture of ferritin-pearlitic steel at −196 °C*, Mater. Sci. Eng. A 686 (2017), pp. 134–141.
[42] G. Oates and J.R. Griffiths, *Mechanisms of cleavage fracture initiation in notched and smooth specimens of 3% silicon iron*, Metal Sci. J. 13 (1969), pp. 341–459.
[43] T. Lin, A.G. Evans, and R.O. Ritchie, *Stochastic modeling of the independent roles of particle size and grain size in transgranular cleavage fracture*, Metall. Trans. A 18 (1987), pp. 641–651.
[44] J.H. Chen and G.Z. Wang, *Change of critical event for cleavage fracture of HSLA steel*, in *Proceedings of 11th International Conference on Fracture (ICF11)*, Vol. 6, paper #2898, Curran Associates, Inc., Red Hook, NY, 2010, pp. 3980–3985.

[45] S.G. Roberts, S.J. Noronha, A.J. Wilkinson, and P.B. Hirsch, *Modelling the initiation of cleavage fracture of ferritin steels*, Acta Mater. 50 (2002), pp. 1229–1244.
[46] J.I. San Martin and J.M. Rodriguez-Ibabe, *Determination of energetic parameters controlling cleavage fracture in a Ti-V microalloyed ferrite-pearlite steel*, Scripta Mater. 40 (1999), pp. 459–464.
[47] B.Z. Margolin, V.A. Shvetsova, A.G. Gulenko, and V.I. Kostylev, *Prometry local approach to brittle fracture: Development and application*, Eng. Fract. Mech. 75 (2008), pp. 3483–3498.
[48] K. Shibanuma, S. Aihara, and K. Suzuki, *Prediction model on cleavage fracture initiation in steels having ferrite-cementite microstructures–Part I: Model presentation*, Eng. Fract. Mech. 151 (2016), pp. 161–180.
[49] W.-S. Lei, *Fracture probability of a randomly oriented microcrack under multi-axial loading for the normal tensile stress criterion*, Theor. Appl. Fract. Mech. 85 (2016), pp. 164–172.
[50] W.-S. Lei, *A generalized weakest-link model for size effect on strength of quasi-brittle materials*, J. Mater. Sci. 53 (2018), pp. 1227–1245.
[51] B.K. Dutta, S. Guin, M.K. Sahu, and M.K. Samal, *Temperature dependency of Berermin's parameters for 20MnMoNi55 material*, Paper#G01/5, in *Transactions of SMiRT 19 Conference, International Association for Structural Mechanics in Reactor Technology*, Toronto, Canada, 2007. Available at https://www.iasmirt.org/transactions/19/G01_5.pdf
[52] B.S. Manjunath, P.V. Durgaprasad, B.K. Dutta, and S.P. Prakash, *Determination of Beremin's parameters for 20MnMoNi55 ferritic steel*, Paper# 129, in *Transactions of SMiRT 21 Conference, International Association for Structural Mechanics in Reactor Technology*, New Delhi, India, 2011. Available at https://www.iasmirt.org/transactions/21/p129.pdf
[53] P.C. Chakraborti, A. Kundu, and B.K. Dutta, *Weibull analysis of low temperature fracture stress data of 20MnMoNi55 and SA333 (Grade 6) steels*, Mater. Sci. Eng. A 594 (2014), pp. 89–97.
[54] G. Qian, W.-S. Lei, and M. Niffenegger, *Calibration of a new local approach to cleavage fracture of ferritic steels*, Mater. Sci. Eng. A 694 (2017), pp. 10–12.
[55] G. Qian, W.-S. Lei, L. Peng, Z. Yu, M. Niffenegger, *Statistical assessment of notch toughness against cleavage fracture of ferritic steels*, Fatigue Fract. Eng. Mater. Struct.